3 SCIENCE AT NSLS-II

The science case for NSLS-II was presented in the proposal submitted for Critical Decision 0 (Approval of Mission Need), which was approved on August 25, 2005. Subsequent to this, in the process of carrying out the conceptual design for NSLS-II, the details and capabilities of the facility have become clearer. In particular, the capabilities of likely beamlines and the science they will enable have become much better defined. Several of these beamlines were examined in some detail, notably those beamlines expected to have especially high scientific impact and those that exploit the high brightness of NSLS-II. In this chapter, we briefly mention some experiments that could be carried out on those beamlines, to provide some context for the conceptual designs discussed later in this document. Note that these examples are not meant to be exhaustive, but rather represent a sampling of the diverse and exciting science that NSLS-II will enable.

3.1 Hard X-ray Nanoprobe

As discussed in Section 11.4, a hard x-ray nanoprobe beamline at NSLS-II will be designed and optimized to enable the production and use of a beam of hard x–ray photons with a minimum beam size in the nanometer range. As such, it will be a world-leading instrument, enabling spatially resolved versions of many powerful structural and spectroscopic x-ray techniques with unprecedented resolution. In particular, it will allow the study of nanomaterials which today play important roles in many diverse scientific fields, opening up a wide range of scientific problems ranging from studying the structure and function of catalytic nanoparticles, to the mapping of strain in buried grain boundaries, to determining the structure of single molecule devices.

Some of the possibilities of such an instrument can be illustrated more concretely by considering a potential experiment on carbon nanotube devices. Carbon nanotubes are among the most studied nano objects. Furthermore, many of the interesting properties of CNTs—metallic or semiconducting transport properties, electroluminescence, photoconductivity, etc.—depend sensitively on their structure. A single-walled CNT can be regarded as a single layer of graphite that has been rolled up into a cylindrical structure.

In general, the CNT is helically wrapped, and a chiral vector can be defined to reflect the way in which the graphite sheet self-registers around the tube. Depending on the chirality [3.1.1], the nanotubes are either metallic or semiconducting. Preparation of CNT samples results in a distribution of nanotube diameters and chiralities, and each fabricated device that randomly selects one from this distribution consequently contains a nanotube with an unknown structure. Currently, the best way to determine the structure of an individual CNT is with electron diffraction [3.1.2, 3.1.3], though this results in damage to the tube. This method also suffers from the drawback that it is very difficult to carry out such a study when the nanotube is buried under a gate electrode structure (as is typically the case), or under a protective barrier, as shown in the device structure in Figure 3.1.1.

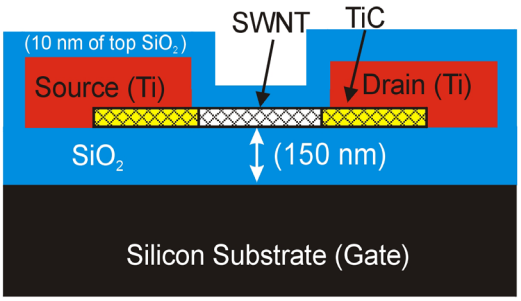

Figure 3.1.1 Schematic of a CNT device in which the nanotube structure is obscured. Such CNTs could be probed with the proposed nanoprobe beamline at NSLS-II.

Figure 3.1.2 shows an SEM image of an actual device. Any protective coatings or support membranes of significant thickness make electron diffraction difficult, so it is almost impossible to compare directly the measured electron transport properties of a given functioning CNT device and its structural properties. As mentioned, a further disadvantage of electron diffraction is that it is a destructive probe of the nanotube structure, so the structural characterization becomes the last step. Although the extent of the damage that an x-ray nanoprobe will induce in a sample has not yet been experimentally resolved, it appears that it will be possible, in at least some cases, to study the structure in situ, with the device in operating conditions. To determine the feasibility of such studies at NSLS-II, the x-ray scattering from a single nanotube has been calculated.

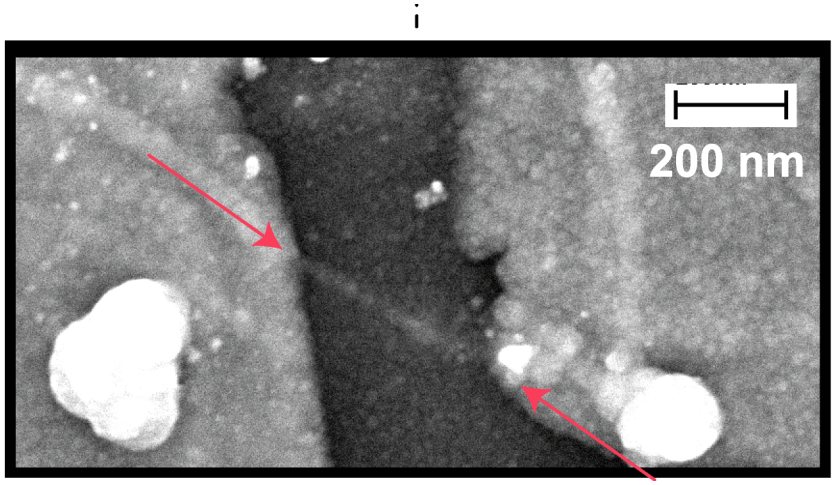

Figure 3.1.2 Scanning electron microscope image of a device.

The model used is illustrated in Figure 3.1.3. A single CNT is illuminated by a perpendicular x-ray polarized parallel to the tube. The diffraction pattern is recorded by a 1024 × 1024 pixel detector array, positioned at a distance d = 20 cm; the pixel area is 100x100 μm^2. The number of counts N recorded by the detector at pixel $\vec{R}$ is given by:

$$N(\vec{R}) = I_{sc}\Delta t = I_0\,\Delta t\,(A_p / A_0)\,(r_0/\mathrm{R})^2\,P(Q)[(\sum_j f_j \cos\phi_j)^2 + (\sum_j f_j \sin\phi_j)^2 \qquad (3.1.1)$$

where I_{sc} is the scattered intensity (number of photons per second impinging on the detector); Δt is the accumulation time; I_o is the incident intensity (number of photons per second impinging on the illuminated area A_0 of the CNT under study); $A_p = R^2\Delta\Omega$ is the (effective) area of the detector and $\Delta\Omega$ is the solid angle that it subtends; $r_0 = 2.8\times10^{-6}$ nm is the classical (Thomson) electron radius; $\vec{R}$ = (X, Y, Z) = (d, mb, nb), where m, n = -215, …, 216 and b = 200 μm specifies the pixel position; $P(Q) = 1 - (\mathbf{e_o}\ ,\ \mathbf{s'}\ )^2$ is the polarization factor, $\mathbf{e_o}$ is the direction of polarization of synchrotron light and $\mathbf{s'} = \vec{R}/\mathrm{R}$ is the direction of scattered light; $fj(Q)$ is the atomic scattering (form) factor of the atom at r_j, calculated ab initio and tabulated in the literature; $\mathbf{Q} = \mathbf{k} - \mathbf{k'}$ is the momentum transfer where $\mathbf{k}$ and $\mathbf{k'}$ are the momentum of the incident and the scattered x-ray photon respectively; and $\phi_j = (Q, r_j)$.

Figure 3.1.3a shows the scattering geometry used in the calculations, with a single-walled (3,3) armchair nanotube illuminated. Figure 3.1.3b shows the resulting diffraction pattern.

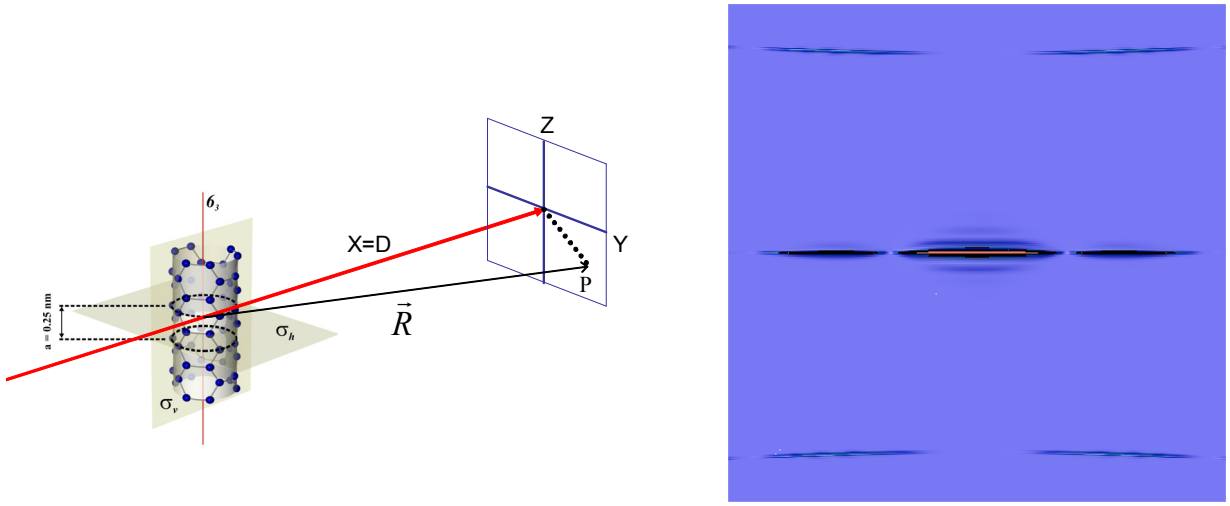

a **b**

Figure 3.1.3 **a**) A single nanotube—here, a (3,3) armchair CNT—is shown illuminated by an x-ray beam, and the diffraction is recorded on a flat screen. **b**) The corresponding x-ray diffraction pattern.

Taking the performance of a 3 m U19 device at NSLS-II and utilizing diffractive optics capable of delivering photons into a 25 nm x 1 nm spot and making reasonable assumptions for the efficiency of these optics and their associated pre-optics, we find that these model calculations give intensities of 10,000 cps in the central maxima and 1,250 cps in the secondary maxima of the diffraction pattern shown in Figure 3.1.3b.

These results illustrate that one will have the sensitivity at NSLS-II to address this important class of problems, understanding the structure of the nanotubes in a real gated device and hence directly connecting their structure to the performance of a given device. Further, the technique will be sensitive to the presence of single dopant atoms on the tube—and to their precise location, as shown in Figure 3.1.4. These capabilities will be revolutionary in the study of such single-molecule devices.

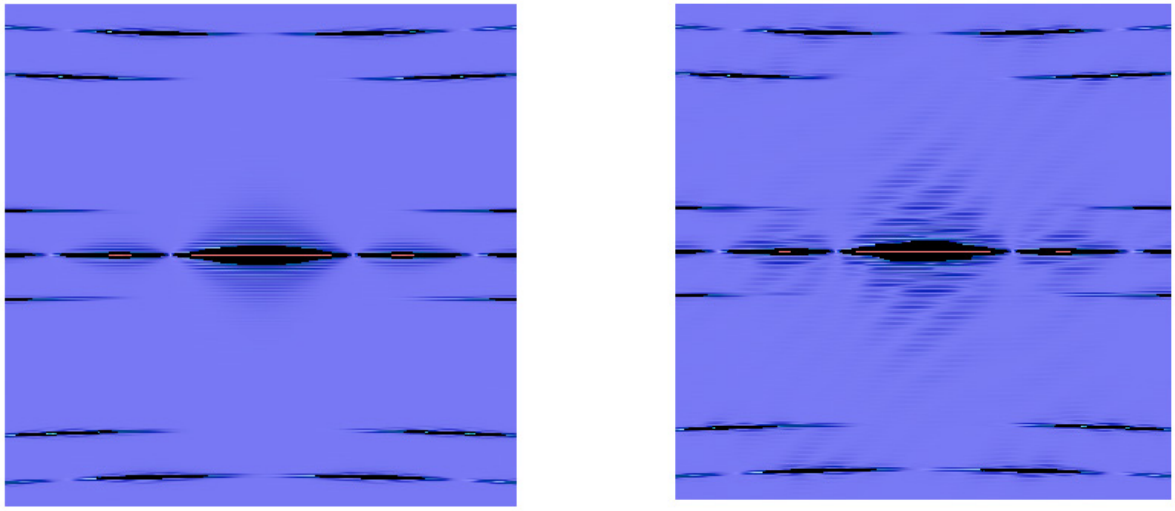

a **b**

Figure 3.1.4 X-ray diffraction from **a**) chiral (4,2) nanotube; **b**) the same, but with one Au atom adsorbed to the side at z = 0.

As a further example of the power of a nanoprobe at NSLS-II, we next calculate the fluorescence from a single Fe atom embedded in a Si matrix. This represents the ultimate limit of a catalytic nanoparticle, which in practice is likely to be made up of tens of atoms.

We first calculate the flux onto a 1 nm spot. To do so, we assume the source properties of NSLS-II with the fully built out complement of damping wigglers, so that the emittance is 0.55 nm-rad. Taking the performance of a 3 m U19 CPMU insertion device occupying a 5 m straight, we calculate the flux delivered onto an optic with a physical aperture of 100 μm. As discussed in Chapter 12, the likely optic for such a beamline is a multi-layer Laue lens (MLL) or a kinoform lens. Both are diffractive, and therefore chromatic, optics; hence, in order to achieve a 1 nm focus they require highly monochromatic beam. In particular, the required bandpass is 3×10^{-5} for a working distance of ~1 mm. Allowing for the reduction in flux associated with this narrow bandpass, together with expected efficiencies for a high-heat-load monochromator, the high-resolution monochromator and the focusing optic, we find that the flux delivered into a 1×1 nm spot is $\sim10^{11}$ ph/s—a very significant number.

Calculating the resulting fluorescence intensity from this flux is relatively straightforward and is given by $I=I_0\omega(\Omega/4\pi)\sigma_{pe}e^{-\mu t}$, where I_0 is the incident flux; ω, the fluorescent yield (=0.35 for Fe), Ω, the collection solid angle of the detector; σ_{pe} the photoelectric cross-section for Fe ($=1.12\times10^{-6}$ nm^2 at 10 keV for Fe K-edge); and the factor $e^{-\mu t}$ accounts for absorption of incoming and outgoing photons in the Si matrix. We ignore this latter factor in these calculations, which is a good approximation for silicon thinner than 1 absorption length (~100 μms at 10 keV). Putting in these numbers, one finds that the fluorescence signal from a single Fe atom is a very respectable ~1,000 cps. Of course there will be background, such as Compton scattering from the silicon, but it should be possible to discriminate against this and thus it will be possible to perform imaging and spectroscopy from a single Fe atom.

In fact, the variation in cross-sections is relatively small for different atomic species. For example, the same calculation for Er L-edge fluorescence for a single Er atom embedded in Si (a problem with relevance to the optoelectronics industry) gives an intensity of 5,000 counts per second with the same assumptions. Thus it should be possible at NSLS-II to perform single-atom imaging and spectroscopy for essentially any atom in the periodic table.

References

[3.1.1] R. Saito, M. Fujita, G. Dresselhaus, and M.S. Dresselhaus, Electronic structure of graphene tubules based on C_{60}, *Phys. Rev. B*. **46** 1804 (1992).

[3.1.2] N. Hamada, S. Sawada, and A. Oshiyama, New one-dimensional conductors: Graphitic microtubules, *Phys. Rev. Lett*. **68** 1578 (1992).

[3.1.3] M. Y. Sfeir, T. Beetz, F. Wang, L. Huang, X.M.H. Huang, M. Huang, J. Hone, S O'Brien, J.A. Misewich, T.F. Heinz, L. Wu, Y. Zhu, and L.E. Brus, Optical Spectroscopy of individual single-walled carbon nanotubes of defined chiral structure, *Science* **312** 554 (2006).

3.2 Coherent X-Ray Scattering

The National Nanotechnology Initiative recognizes the rapidly growing importance of nanostructures, and the potential that future developments in this area have for major breakthroughs in the fundamental and applied sciences and in technology. On this scale—as on all others—imaging is clearly one of the most important characterization tools to connect form with function. In the previous section, real-space imaging was discussed. Coherent x-ray scattering offers an attractive alternate route to solving the structure of nanoparticles with very high spatial resolution—by working in reciprocal space, illuminating the structure with coherent light, and inverting the resulting image. The technique places very high demands on the

coherent flux from the source and as a result NSLS-II is expected to provide an important advance in the field.

On the highest resolution scale, x-ray crystallography provides excellent 3D representations of the molecular structure for materials that can be crystallized. For noncrystalline samples less than 50 nm thick, aberration-corrected transmission electron tomography promises to provide 3D images at 0.1 nm resolution. X-ray microtomography is presently capable of 3D imaging at 60 nm resolution, and is likely to develop further to resolutions of 30 nm. However, it is limited to thin samples at these high resolutions, due to depth-of-field effects. There is, therefore, a significant gap, in that none of these techniques can image samples thicker than a hundred nm and with high spatial resolution.

Coherent diffractive imaging promises to be a powerful microscopic method for imaging noncrystalline or finite-size objects at high spatial resolution, in thick samples and beyond the resolution limit set by x-ray optics. We show here that for very radiation-resistant materials, true atomic imaging with a resolution as small as 0.1 nm may be possible using NSLS-II.

The idea is to determine the spatial distribution of electron density $\rho(r)$ in a noncrystalline sample by measuring its far-field coherent x-ray diffraction pattern. It is analogous to x-ray crystallography, but with two important distinctions. First, the diffraction pattern is a continuous function in reciprocal space for a noncrystalline or finite-size sample, as opposed to discrete Bragg peaks for a bulk crystal. This allows the application of an iterative oversampling phasing algorithm for phase retrieval and structure determination. Second, the method requires an intense coherent x-ray beam incident on the sample to preserve the phase information in the diffraction pattern and overcome the lack of periodicity in the sample.

Here we summarize the requirements on the source for imaging an object of size L with spatial resolution d. One can show that the required incident coherent intensity, I_o (ph/s/cm^{-2}), for determining the reconstructed 3D structure with acceptable signal to noise in time Δt is given by

$$I_o\Delta t = 20\pi^3/(3r_o^2Ln_o^2d^3f^2\lambda^2) \approx (3\times10^{-20}\ gm^2/cm^2)/(Ld^3\lambda^2\rho^2) \qquad (3.2.1)$$

where n_o is the atom density (atoms/cm^3), f is the scattering amplitude (~Z, the atomic charge), λ is the wavelength, and ρ is the mass density (gm/cm^3). This shows that the coherently scattered signal scales with ρ^2 and d^3 and is proportional to sample thickness, L. Table 3.2.1 gives $I_o\Delta t$ required to image a 1 μm^3 volume with 1 nm resolution for materials having a range of densities from light (carbon) to heavy (gold). The dose equivalent is also given in Table 3.2.1 and discussed below.

Table 3.2.1 Coherent Diffraction Measurement Considerations at NSLS-II. Required coherent flux density, equivalent dose, and measurements times for unfocused and focused radiation from NSLS-II, for imaging a 1 μm^3 volume of different materials with 1 nm resolution.

Material	$I_o\Delta t$ (ph/μm^2)	Dose (Gray)	Measurement Time NSLS-II Unfocused	Measurement Time NSLS-II Focused
Carbon (Z = 6)	7.1 x 10^{12}	4.3 x 10^9	14 hours	20 seconds
Cobalt (Z = 27)	1.6 x 10^{11}	3.0 x 10^9	19 minutes	0.4 seconds
Ruthenium (Z = 44)	8.7 x 10^{10}	2.0 x 10^9	10 minutes	0.2 seconds
Gold (Z = 79)	3.5 x 10^{10}	0.95 x 10^8	4 minutes	0.1 seconds

With NSLS-II, the coherent flux at 8 keV will be 6×10^{12} ph/s after the Si monochromator, which will provide the appropriate longitudinal coherence. The transverse coherence lengths will be 65 μm and 819 μm in the vertical and horizontal, respectively, at 25 m from the source. Thus, the incident coherent intensity in the required bandwidth will be 1.4×10^8 ph/s/μm^2. The times required to collect the diffraction patterns for the examples above range from 4 minutes to 14 hours.

The incident coherent intensity can be increased by focusing while still meeting the coherence requirements. This is because the divergence angle of the coherent radiation from NSLS-II is 14 μrad in the horizontal and 3.2 μrad in the vertical, whereas the smallest detection angle is $\lambda/(1.4L) = 110$ μrad. For a focused beam size of about 4L, the gain in coherent intensity for the case of 1 μm is a factor of about 2600. This reduces the time to measure the diffraction patterns to from 0.1 to 20 seconds, as shown in Table 3.2.1.

The requirement of an intense x-ray beam for coherent diffraction measurements may cause radiation damage to the sample, which would ultimately limit the tolerable dose, and thus the achievable spatial resolution. Table 3.2.1 shows the required dose depends only weakly on composition and density.

Several studies have shown that radiation-damage effects in biological specimens at a given dose depend on the spatial resolution of interest. At atomic resolution, it is commonly accepted that a dose of 2×10^7 Gy is enough to destroy crystalline order in protein crystals. At much lower resolutions, however, much higher x-ray dosages of 10^{10}-10^{11} Gy can be tolerated at cryo-temperatures. These radiation-damage limits are purely empirical, and are for biological specimens only. The x-ray radiation tolerance for inorganic materials has been less well studied, but indications are that it can be a factor of 100, or more, higher than for biological materials.

Table 3.2.2 shows the required dose and measurement times for imaging such a $(10\ \mu m)^3$ volume of different materials with 0.3 nm resolution. Carbon is included since, for example, carbon nanotubes have been shown to be very radiation resistant – at least 100 times higher than for biological materials. A $(10\ \mu m)^3$ volume of carbon nanotube bundles could thus be imaged with 0.3 nm resolution. Such experiments will complement the single molecule diffraction experiments discussed above. The required time is reasonable, at a few minutes or less for most materials. It should be noted that no losses have been taken into account for the monochromator (other than accounting for its bandwidth), focusing optics, or beamline windows, and the detector quantum efficiency has been assumed to be 100%. In addition, the finite readout and storage rate for area detectors has been neglected. In practice, these losses, plus the overhead from detector readout, might increase the measurement time by a factor of ~ 5. These will combine to give measurement times of ~ 10 minutes, which are still reasonable.

Table 3.2.2 Required Coherent Flux Density, Equivalent Dose, and Measurement Times. Values are for unfocused and focused radiation from NSLS-II, imaging a $(10\ \mu m)^3$ volume of different materials with 0.3 nm resolution.

Material	$I_o \Delta t$ (ph/μm²)	Dose (Gray)	Measurement Time NSLS-II Unfocused	Measurement Time NSLS-II Focused
Carbon (Z = 6)	2.6×10^{13}	1.6×10^{10}	52 hours	2.2 hours
Cobalt (Z = 27)	5.9×10^{11}	1.1×10^{10}	1.2 hours	2.9 minutes
Ruthenium (Z = 44)	3.2×10^{11}	7.4×10^{9}	37 minutes	1.5 minutes
Gold (Z = 79)	1.3×10^{11}	3.5×10^{8}	15 minutes	37 seconds

This analysis has shown that for radiation-resistant nonbiological material, such as nanostructures, nanocomposite materials, magnetic materials, and others, the physical, chemical, and magnetic imaging of materials with atomic spatial resolution will be possible at NSLS-II.

One example of an area where this will have tremendous impact is that of inorganic open-framework materials, such as zeolites. These porous materials can have superior catalytic or sorption properties. The latter might be especially important for hydrogen storage applications. These materials often occur as powders with poor crystallinity, so conventional x-ray diffraction can have limited applicability. In addition, their catalytic activity is often due to other species, such as transition metal atoms, absorbed on their high surface area interior. These active atoms are often heterogeneously distributed throughout the porous material, so, once again, conventional diffraction is ineffective.

For example, nickel succinate is a 3D porous open framework structure. The pores are 0.8 nm in diameter and the pore–pore spacing is 2.3 nm. Imaging this structure with 0.3 nm resolution using NSLS-II will clearly reveal the pore structure and atoms lining the pore surface.

Some other applications of coherent diffractive imaging in the material sciences include: 1) imaging the complex tangle of dislocation lines that are responsible for work hardening; 2) imaging the cavities inside duplex steels that are responsible for their very high uniform extension; 3) 3D imaging defect structures in magnetic multilayers; 4) tomographically imaging misfit dislocations at interfaces, free of the thin-film elastic relaxation processes that distort the images obtained by transmission electron microscopy; 5) imaging the 3D arrangement of Orowan dislocation loops which, by entanglement with particles, provide the dispersion-hardening of copper alloys; 6) imaging precipitates in metal–matrix composite materials; and 7) imaging electronic or spintronic device elements for future computing schemes, such as quantum computing.

For very radiation-resistant materials, true atomic imaging with a resolution as low as 0.1 nm may be possible. With NSLS-II, this will require measurement times on the order of 10 minutes × $(3)^3$, or about 4.5 hours for a 10 μm^3 sample, which is not unreasonable.

3.3 X-Ray Photon Correlation Spectroscopy (XPCS)

X-ray photon correlation spectroscopy also utilizes the very high coherent flux at NSLS-II, in this case to probe the equilibrium or steady-state dynamics of condensed matter. In this endeavor, the XPCS technique offers the significant strengths of being able to study length scales shorter than can be achieved with optical techniques and longer time scales than can be achieved via neutron scattering. Even on optically accessible length scales, it permits the study of opaque and metallic samples, presenting new opportunities for studies of colloidal and other soft-matter systems.

XPCS involves creating a partially coherent x-ray beam, which is allowed to impinge upon a sample. The dynamics of any fluctuations within the sample are then determined by characterizing the intensity autocorrelation function, $g_2 = g_2(Q,t)$, of the resultant x-ray speckle pattern versus delay time (t) and wave vector (Q). In a certain sense, this may be thought of as the time-resolved counterpart to coherent diffraction discussed above. Importantly, the quantity $g_2(Q,t)$ is related to the sample's normalized intermediate scattering function (ISF) $[f(Q,t) = S(Q,t)/S(Q,0)]$ via $g_2(Q,t) = 1+A[f(Q,t)]^2$, where A is the optical contrast. The ISF (equivalent to the sample's Q- and t-dependent density–density autocorrelation function) is a quantity of central interest for any condensed matter system, and is usually key in comparing theory to experimental results.

However, PCS is much more challenging with x-rays than with light. This is due to a combination of the fact that there are many fewer photons in x-ray beams from even the brightest synchrotrons than from laser sources, and the fact that x-ray scattering cross-sections are invariably many times smaller than light scattering cross-sections. As a result, the crucial aspect of any XPCS experiment is generally the signal-to-noise ratio.

The XPCS SNR is linearly proportional to the source brightness. Since the brightness of NSLS-II will exceed by a factor of 30 that of any source in existence today, the corresponding SNR will be about a factor of 30 higher. NSLS-II will drive a revolution in the kinds of samples that will be accessible to XPCS studies. Interestingly, while the SNR scales linearly with brightness, it only scales as the square-root of the sample time (which should be a few times smaller than the sample's correlation time). It follows that for samples of a given scattering strength, meaningful XPCS measurements will be possible at NSLS-II on time scales that are about 10^3 times faster than currently possible anywhere. Since the current state-of-the-art for diffuse scattering measurements (not from liquid crystal Bragg peaks, or surface specular reflection) corresponds to sample times of about 1 millisecond, we expect time resolutions at NSLS-II of 1 microsecond or less to be

feasible, which will enable entirely new science. Indeed, with a time resolution of 0.1 microseconds, it may be possible, in favorable circumstances, to overlap with neutron spin echo measurements.

There are several classes of XPCS experiments that will be possible at NSLS-II but are impossible at current facilities. These include:

Membrane Dynamics. Studies of the dynamics of membrane-based complex fluid phases, consisting of oil–water and an amphiphilic surfactant. Such phases—including the sponge phase and the bicontinuous microemulsion phase, for example—have been the subject of intense interest over the past 20 years, not least because of their possible utility in enhanced oil recovery applications. There are detailed predictions for the equilibrium dynamics of such phases for the wave vectors most characteristic of these materials, namely wave vectors at and near the peak of the static scattering. However, these dynamics are typically too slow for neutron spin echo (NSE) measurements and occur at wavevectors that are too large for optical studies. The faster time scales made accessible by the enhanced brightness of NSLS-II will enable XPCS studies to test these predictions.

Nanoparticles in Suspension. Studies of the collective dynamics of suspensions of nanoparticles. At NSLS-II, it will be possible to study fluctuation dynamics of smaller nanoparticles than is possible now. This will, for example, permit studies of the motions of nanoparticles confined within block copolymer matrices, or on surfaces. Such studies will be critical in understanding the processes underlying how small particles self-assemble into potentially, technologically useful structures. Especially interesting will be studies examining mixtures of differently-sized nanoparticles of differing compositions, which can self assemble into a variety of different structures, depending on their relative sizes, and which it may be possible to selectively probe via anomalous scattering methods.

Polymer Dynamics. A longstanding question in polymer science concerns so-called *reptation*, which is the process by which polymers in an entangled polymer melt diffuse. The enhanced brightness of NSLS-II will permit XPCS studies on shorter length scales than is now possible, allowing such studies to critically examine the reptation model and relaxations associated with reptation in polymer melts in a much more direct fashion—by actually looking at the polymer motion—than has been possible previously.

Surface Fluctuations. Surface XPCS studies carried out at NSLS-II will probe shorter length scales and faster time scales than are possible now and will therefore elucidate the dynamical behavior of thin liquid and polymer films, and permit definitive answers to questions concerning the role of surface roughness in quenching dynamical fluctuations, or of a polymer's radius of gyration in determining a polymer thin film's capillary mode spectrum.

3.4 Small Angle X-Ray Scattering (SAXS)

Small angle x-ray scattering can provide information on sample inhomogeneities in the nm range, providing, for example, information about the shape and size of macromolecules, characteristic distances of partially ordered materials, pore sizes, etc. SAXS is capable of delivering structural information on macromolecules between 5 and 25 nm, and of repeat distances in partially ordered systems of up to 150 nm. USAXS (ultra-small angle x-ray scattering) can resolve even larger dimensions. Present trends in the field are toward extending the technique both to longer length scales and, through the use of flow cells, to faster time scales, a trend that will accelerate with the availability of the high-brightness beams at NSLS-II. In this section we provide several examples of research areas in which a state-of-the-art SAXS instrument at NSLS-II will have significant impact.

3.4.1 Dynamical Events in Biological Macromolecular Solutions

Macromolecular crystallography has provided much of our knowledge about the function and interaction of various proteins and other biomolecules. However, these functions often depend on flexibility of the molecule, and on environmental parameters such as pH and ion concentration. Furthermore, in cases where the molecule is flexible or is insoluble in water (such as membrane proteins), crystallization may be difficult. In such cases, structural studies in solution, where flexibility is natural and solution parameters can be controlled, can complement or even replace crystallographic studies.

In this context, there have been two recent developments in the instrumentation and data analysis of small angle solution scattering, namely, micro-fabricated flow cells and the low-resolution shape reconstruction algorithms. These advances, combined with NSLS-II beams, will provide new insights into the function, control, and dynamics of individual macromolecules and large molecular complexes.

Micro-fabricated flow-cell mixer is a technology that allows sub-millisecond-resolution time-resolved x-ray scattering measurements. In particular, the continuous-flow diffusion mixer (Figure 3.4.1) [3.4.1, 3.4.2] has the potential to provide μs time-resolution. This device produces thin laminar flow sheets of solutions. Dynamical events are triggered as the solutions mix by diffusion between the solution sheets, and one follows the events in time by measuring at different positions downstream. For instance, to generate a protein-folding event, denatured protein is injected into the central channel, sandwiched between buffer solutions. As the protein and buffer solutions flow downstream, the denaturant diffuses out of the protein layer. Once the denaturant concentration drops below a threshold, the protein folds back to its functional conformation. The solution mixer can also trigger other biochemical reactions by a similar mixing of reactants.

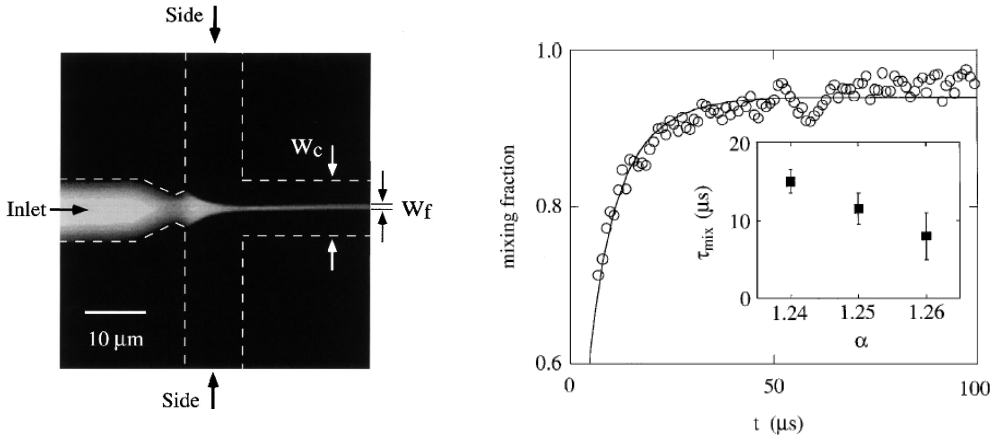

Figure 3.4.1 Fluorescence image of a continuous-flow cell, (left) and its intrinsic time resolution (right). Time resolution is on the order of ~10 μs [3.4.1]. X-ray studies in such cells will be possible at NSLS-II. The fluorescein-labeled inlet flow is bright in the image. Currently, limited by x-ray beam size and intensity, the mixers used for x-ray experiments are larger (50–100 micron channels) and the time resolution is on the order of 1 millisecond.

However, the potential of solution-mixers for SAXS measurements can only be fully realized when the device is used with very high brightness x-ray beams. This is because the time-resolution that the mixers can provide is limited by the beam size. An intense and small beam not only allows a smaller overall dimension of the solution layers and reduces sample consumption, but also improves the time resolution. Note that radiation damage effects are mitigated because the sample is continually renewed by the flow.

The second development is a handful of shape determination algorithms [3.4.3, 3.4.4] that have excited renewed interest in solution scattering. The basic idea behind these methods is that although the molecules in solution are randomly oriented and much of the structural information is lost in the isotropic average, some information that is characteristic to the shape envelope of the biomolecules remains in the measured one-

dimensional scattering curve. This may suffice to define a low-resolution shape envelope. In many cases, the subunits that make up a protein complex, for example, are rigid and their atomic structures are known. Solution scattering can then provide a useful tool for putting the pieces of this puzzle together to reveal the functional structure of the protein complex; by knowing the shape of components, one reduces the degrees of freedom in the model, and the overall shape determination becomes much more reliable.

Solution mixers are already being used, in combination with size characterization provided by simple SAXS analysis, to study protein folding on a time scale of milliseconds. With smaller, brighter x-ray beams to improve the time-resolution and the more sophisticated data analysis outlined above, low-resolution movies may be created to capture events such as the assembly and functioning of molecular machines, for the first time.

3.4.2 Structures in Model Membranes Submerged in Water

Many of the most intriguing biological processes, such as cell recognition, signal transduction, chemical sensing, and transportation, take place in the membranes of cells and organelles. Yet, progress in membrane research has been painfully slow, mainly because of the difficulty of crystallizing membrane proteins and a lack of alternative structural characterization tools.

Progress is being made slowly in preparing model systems for x-ray structural studies of biological membranes. A very promising model system is substrate-supported single bilayers [3.4.5] that resemble native cell membranes. A lipid bilayer of biologically relevant composition can be spread on a flat substrate so that Grazing Incidence SAXS (GISAXS) can be carried out to probe the structures embedded in the bilayer, such as membrane proteins. This technique applies to both fluid-like membrane structures and 2D membrane protein crystals, if such crystals are available [3.4.6].

It is important to note that lipid bilayers are stable only in an aqueous environment and disintegrate instantly in air because of the lower surface energy when the hydrophobic lipid chains are exposed to air. While keeping the membrane under water is advantageous because the solution provides many possibilities to control the membrane structures, it also leads to experimental problems because of absorption issues and because it gives rise to significant background scattering. The experiments therefore must be done with high energy x-rays (>20 keV for less x-ray absorption) and relatively small samples (<1 cm long) illuminated at grazing incidence. The latter implies the need for a small beam size in the direction perpendicular to the model membrane. For instance, at the water–Si interface, the critical angle is 0.064º, at 20 keV. The vertical beam size must therefore be less than 10 microns in order not to overfill a sample that is 1 cm long. In the case of semi-crystalline structures, the beam footprint may need to be limited to be comparable to the horizontal beam size (<1 mm) so that in-plane powder average can be effectively performed. The beam height in this case will therefore need to be less than 1 micron.

These requirements present instrumentation challenges for scattering experiments on model membranes under water. Not only must the x-ray beam be intense enough so that the scattering from the extremely thin (~5 nm thick) lipid film can produce high-quality data, but the beam divergence must also be smaller than usual so that the instrument can access the same q-range as instruments operating at lower x-ray energies (note that for the same scattering angle, the q value is inversely proportional to x-ray energy). Routinely carrying out these experiments will only be possible at NSLS-II.

Studies on lipid membranes under water are just beginning (Figure 3.4.2) [3.4.7, 3.4.8], with the promise of emulating bulk SAXS and crystallography studies. At NSLS-II, they will provide a generic tool for studying membrane structures that are relevant to biology.

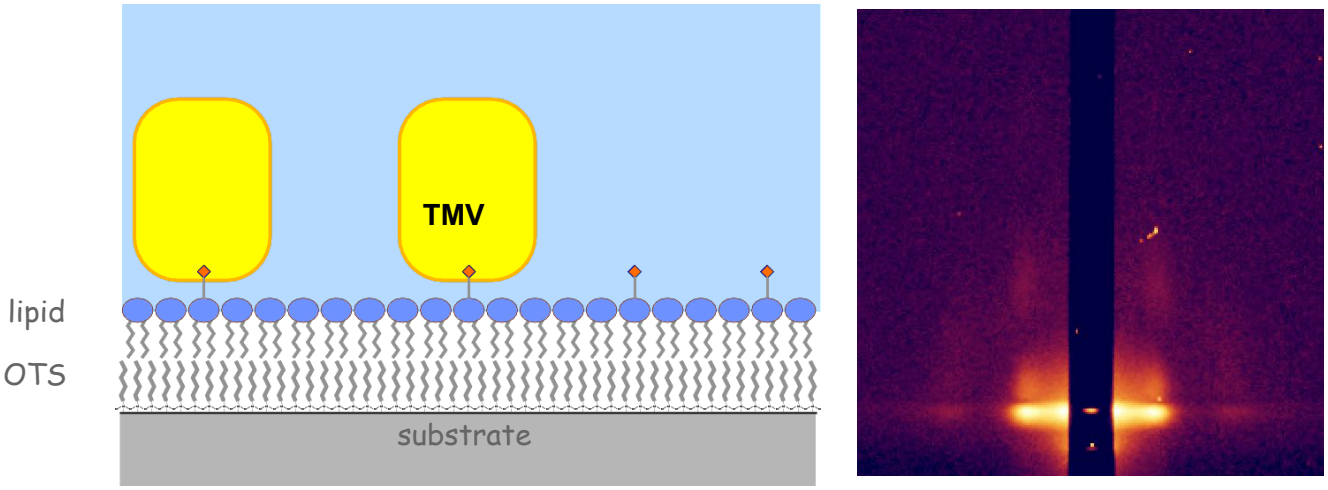

Figure 3.4.2 Schematic of self-assembled arrays of tobacco mosaic virus adsorbed onto a lipid film under water (left), and (right) GISAXS pattern from the formed arrays [3.4.8]. Membrane proteins also can be attached to the lipid film, provided the appropriate ligands (red dots in the schematic) in the lipid layer provide anchorage. Currently, the data quality is limited by the x-ray intensity at the sample and the divergence of the x-ray beam.

3.4.3 Molecular and Supra-Molecular Organization in Micro-Textured Materials

Microbeam-based techniques, such as microbeam diffraction and microbeam x-ray fluorescence, in effect provide a scanning probe microscope for studying the internal textures in materials. Unfortunately, producing a microbeam inevitably requires focusing the beam and thus increasing beam divergence, making scanning SAXS measurements problematic. However, as a result of the exceedingly high brightness at NSLS-II, the x-ray beam divergence will remain low even after focusing and scanning. SAXS studies of textures with underlying supra-molecular-scale structures, as in polymers and liquid crystals, will become possible.

There are two areas in which microbeam SAXS will be very useful. The first is for studies of biomaterials, such as bones and hair, which exhibit hierarchical structures. Microbeam SAXS/WAXS reveals the organization of the material on the molecular and supramolecular levels and helps to elucidate the relationship between the structure and the properties of the materials, as, for instance, in diseased tissues.

The second area is in-situ characterization of materials used in devices. Soft materials such as liquid crystals and polymers do not exhibit long-range structural order and their structures very often depend on the local environment, such as the presence of interfaces and temperature distribution. Therefore they cannot be studied as bulk materials. High energy x-rays may also prove useful in this area, since these materials are often buried under other materials.

References

[3.4.1] J.B. Knight, et al., *Phys. Rev. Lett.* **80** 363 (1998).
[3.4.2] L. Pollack, M.W. Tate, A.C. Finnefrock. C. Kalidas, S, Trotter, N.C. Darnton, L. Lurio, R.H. Austin, CA Batt, S.M. Gruner, and S.G.J. Mochrie, *Phys. Rev. Lett.* **86** 4962 (2001).
[3.4.3] D.I. Svergum, *Biophys. J.* **76** 2879 (1999).
[3.4.4] P. Chacon, F. Moran, J.F. Diaz, E. Pantos, and J.M. Andreu, *Biophys. J.* **74** 2760 (1998).
[3.4.5] E. Sackman, *Science* **271** 43 (1996).
[3.4.6] H. Tahlberg, D. Fotiasis, S. Scheuring, H. Remigy, T. Braun, K. Mitsuoka, Y. Fujiyoshi, and A. Engel, *FEBS Lett.* **504** 166 (2001).
[3.4.7] C.E. Miller, J. Majewski, T. Gog, and T.L. Kuhl, *Phys. Rev. Lett.* **94** 238104 (2005).
[3.4.8] L. Yang, M. Fukuto, and S. Wang, in preparation.

3.5 Inelastic X-Ray Scattering (IXS)

The previous sections discussed the use of the very high brightness of NSLS-II to probe the structure and dynamics of condensed matter. In this section, we discuss a technique that utilizes the very high flux to study dynamics on very fast time scales (ps to fs) by working in the energy domain—namely, inelastic x-ray scattering.

IXS is a momentum-resolved technique for studying dynamics and excitations in condensed matter systems. Of increasing importance, IXS has been used to study excitations ranging from phonons in solids, to sound modes in liquids and polymers, to plasmons in simple metals, to complex electronic excitations in strongly correlated electron systems. Further, there are many new, as yet largely unexplored, areas to which the technique could well make important contributions, including surface dynamics, excitations in extreme environments, time-resolved studies, and non-equilibrium dynamics.

As a technique that probes one of the fundamental response functions of condensed matter, namely $S(q, \omega)$, IXS is an extremely powerful method for addressing some of the most important questions in science today. Its principle limitation to date has been the dearth of active instruments in the world, and the very low count rates achievable on such instruments. Despite these limitations, IXS has the intrinsic advantages of a weak cross-section (so that multiple scattering effects are negligible) and the ability to study very small samples. This latter attribute has been used, for example, to study phonons in high Tc compounds (in MgB_2, in plutonium micro crystals, etc.), for which larger, neutron-sized crystals are simply not available. Further, there is no need to deuterate samples, as there is for inelastic neutron scattering from many soft-condensed-matter systems. As a result, given sufficient availability of instruments and reasonable count rates, IXS should have an impact at least as large as that of triple-axis neutron spectrometry, its direct analog. IXS beamline(s) at NSLS-II, as discussed in Section 11.5, will feature unprecedented resolution and count rates and thus are expected to offer the potential for high scientific impact.

As Figure 3.5.1 shows, IXS offers the ability to probe excitations over a range of energy and momentum transfers, q, that cannot be studied with other techniques. For instance, light scattering with an energy of ~1 eV has a maximum momentum transfer of about 10^5 cm^{-1}; much smaller than a typical Brillouin zone boundary, which is ~10^8 cm^{-1}. While neutrons can reach higher q values, they have only an extremely weak coupling to electronic excitations, and are therefore not ideal probes of these excitations. Electron Energy Loss Spectroscopy is very sensitive to surface modes, and is thus complementary to IXS, which observes primarily volume modes. Further, IXS has the advantage of a wider range of accessible momentum transfers, since EELS is limited by multiple scattering effects to relatively small momentum transfers. In addition, EELS requires high vacuum and so is incompatible with certain environments, such as liquids or systems under high pressure. It is also incompatible with strong electric or magnetic fields.

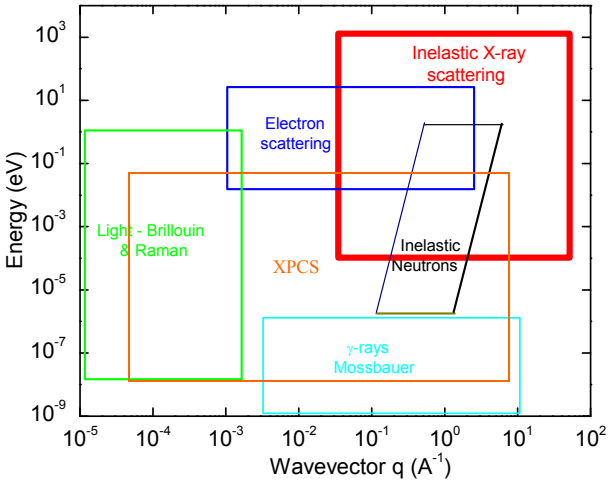

Figure 3.5.1 Probing the Dynamic Response of a System. IXS (red outlined area) covers a range of wave-vector and energy transfers that are inaccessible with other techniques.

With the inherent strengths of the technique and the increasing brightness of synchrotrons, IXS has grown as a technique, with impact in diverse fields of science. NSLS-II will play a key role in pushing this trend still further. Below, we discuss two energy transfer regimes.

3.5.1 Very High-Resolution Inelastic X-Ray Scattering

The capabilities of NSLS-II will allow for a dramatic improvement in the state-of-the-art for IXS instruments, and indeed this is one of the principal goals for the facility. A novel feature of the proposed inelastic spectrometers at NSLS-II is that they will operate at high energy resolutions but utilize moderate photon energies—in contrast to the existing instruments around the world that operate with photon energies on the order of 20 keV and higher.

It is natural to ask what the implication of operating at lower photon energies is on the expected phonon intensities. A useful estimate of the phonon x-ray cross-section has been provided by Sinn [3.5.1], who estimated that the intensity of single phonon scattering for small momentum transfers, q, in a mono-atomic elemental solid was

$$I = I_0 \frac{r_0^2 \hbar^2 c^2}{2e} (\delta q)^2 \frac{1}{E_i^2} Z^2 n_0 \ell_{abs} \frac{k_B T}{M v^2} \ , \qquad (3.5\text{-}1)$$

where the symbols have their usual meaning, the sample is one absorption length, ℓ_{abs}, thick (which results in the largest possible signal) ν is the speed of sound in the solid, and n_0 is the number density in the solid. From this, if one compares two instruments with the same momentum resolution, δQ (note that $\ell_{abs} \propto E_i^3$), one finds that, to a reasonable approximation, $I \propto E_i$, assuming that in all cases the sample is 1 absorption length thick. Thus, operating at 10 keV instead of 20 keV will result in a cross-section that is smaller by a factor of two. However, as noted in Section 11.5, the performance of the source, as measured in ph/s/meV, is significantly better at lower energies than at high energies (see Figure 11.5.2). That is, the pre-factor I_0 (the incident intensity) is significantly higher, and this more than makes up for the reduction in cross-section.

For the spectrometer based on the asymmetric optics scheme proposed in Section 11.5, one can estimate the flux on the sample from a 3 m U19 CMPU device at NSLS-II. Taking into account expected efficiencies of the various focusing optics and the high-resolution monochromator itself, one obtains a flux on the sample of ~10^9 ph/s at 9.1 keV with a 0.1 meV bandpass. This compares favorably with existing high-resolution inelastic spectrometers. For example, the new instrument at Sector 30 at APS delivers ~10^9 ph/s on the sample at 1.5 meV energy resolution from a 4.8 m U30 device, and BL35XU at SPring-8 delivers ~5×10^9 ph/s on the sample at 1.5 meV resolution from a 4.5 m U35 undulator source. Thus the incident intensity is expected to be comparable to existing instruments, but with more than an order of magnitude better energy resolution. Note also that because the absorption length is smaller at these lower energies, only very small volumes of sample will be required.

As an example, consider the case of indium, a low-temperature superconductor (T_C = 3.4 K). It has an absorption length of 10 μm at 10 keV. With the new instrument discussed here, one could measure the phonons in indium relatively easily. Equation 3.5-1 predicts count rates at small q will be ~5 cps (and this will increase at larger momentum transfers, since the phonon cross-section varies as q^2). Note that a lower limit for detectable count rates in an inelastic experiment is typically ~5×10^{-3}, given by the electronic noise level of the detector. Thus, this intensity (5 cps), at this resolution, should provide the sensitivity to observe subtle changes expected in phonon lifetimes as the superconducting state is entered and scattering pathways are removed by the opening of the superconducting gap. This in turn sheds direct light on the electron–phonon coupling which controls the superconducting pairing mechanism. With this understanding in hand, experiments at NSLS-II will turn to high-temperature superconductors for which the pairing mechanism

remains a mystery. These ultra-sensitive phonon measurements should reveal unambiguously if phonons are indeed involved in the superconducting state of the high-temperature superconductors.

There are numerous other systems that require very high-resolution measurements of dynamical modes. These include:

Structural phase transitions. These transitions are frequently driven by a phonon mode going "soft," that is, driven toward zero energy. In cases where such soft modes are present, one needs to measure the phonon softening to as low an energy as possible. As the transition is approached, the phonon energy becomes progressively lower. In addition, frequently there is also elastic scattering appearing, so that very high energy resolution is needed to separate the phonon from this so-called "central peak." An example of a relevant current problem in this field is that of shape memory alloys, and a subset of the general problem of martensitic phase transitions. These latter—which occur in steel—have been dubbed the world's most economically important metallurgical transition [3.5.2]. While shape memory alloys underlie many technologically relevant applications, including military, medical, safety, and robotics applications, the details of the physics that underlies these transitions remain to be explored. The IXS instrument at NSLS-II proposed here, with the ability to study phonons at very high resolution and in very small samples, will make dramatic contributions to this field.

Dynamics of CDW transitions. **C**harge **d**ensity **w**aves form in a wide variety of systems. There are at least two mechanisms that can drive such a transition. One is due to electron–phonon interactions, as, for example, in the classic CDW system, $NbSe_3$, and the other is due to electron–electron interactions in strongly correlated systems, as may be the case in the transition metal oxides, for example. CDWs are characterized by a two-component order parameter, given by the amplitude and phase of the density wave. There are excitations associated with each component, known as amplitudons and phasons, respectively. However, these are excitations of the electronic system, and inelastic neutron scattering is thus not well suited to their study. Inelastic x-ray scattering is thus the probe of choice. However, phasons are gapless and consequently have low energies at small momentum transfers; to study them will require extremely high resolution, coupled with high intensity.

Thermoelectric materials. These are materials which produce a voltage difference across the material in the presence of a temperature difference (and vice versa). They thus offer great potential in future energy applications. However, while many materials, including simple metals, are thermoelectric, most produce only a very small voltage for a given gradient. To be efficient, such materials must have very low thermal conductivity. A great deal of activity is currently underway to find good ways of doing this. One method is to modify the structure so as to reduce the phonon lifetimes by disorder or by putting "rattlers" into an open structure. Nanostructured materials offer particular promise in this regard. However, to date very little has been done to measure phonon linewidths in these materials, or even to study them theoretically. IXS at NSLS-II will make it possible for these linewidths to be studied, even in very small samples, and for parametric studies to be performed.

3.5.2 Moderate Resolution Inelastic X-Ray Scattering

In addition to the very high-resolutions discussed above (1 meV and 0.1 meV), NSLS-II will also have a very large impact in the science carried out at more moderate energy resolutions. With moderate resolution, defined here as 10 to 100 meV, one is able to probe the dynamics of electronic excitations as well as higher energy phonons. These electronic excitations include collective modes, such as plasmons, single-particle-type excitations such particle-hole pair creation in a Fermi-liquid, and excitations across various gaps (such as the charge transfer gap, Hubbard gap, superconducting gap, or band gap). The energy, dispersion, and lifetime of such excitations play an enormously important role in determining the properties of essentially all of the materials of current interest in condensed matter physics.

In addition, in many cases it is possible to carry out resonant IXS (RIXS) in which the incident energy is tuned to the energy of a particular excitation at an absorption edge. This type of scattering can increase the cross-section by more than two orders of magnitude in certain cases, greatly extending the applicability of the technique. Such resonant scattering also offers atomic and initial state selectivity that allows for much additional information about an excitation, which can be crucial to identifying the nature of the excitations.

Much of the current work has focused on copper-based compounds, including 2D systems containing copper oxide planes, and 1D chain compounds. One area of great interest is the study of Mott insulators such as the high temperature superconductor parent compounds, in an attempt to understand how the Mott gap and other excitations evolve as a function of doping. An understanding of this area is important for studies of the high temperature superconductors in particular, and many highly correlated systems in general. As an example of this work, M. Z. Hasan et al. [3.5.3] have looked at the evolution of the Mott gap with doping dependence in both hole and electron-doped superconductors, and find that the phase diagram for these systems is directly related to the measured Mott gap, indicating a relation between the pseudogap and the Mott charge gap.

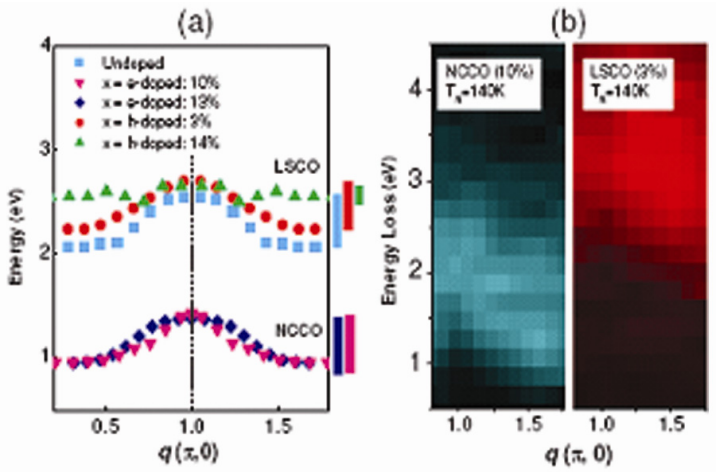

Figure 3.5.2 **a**) Mott gap in doped cuprates. **b**) Systems with the same Neel temperature but different doping.

From M. Z. Hasan, et al. [3.5.3]

As discussed in Section 11.5, the proposed medium energy resolution instrument will feature a number of significant advances over the existing instruments. Principal among these will be the higher intensities resulting from the larger fluxes available at NSLS-II, and improved resolution and throughput resulting from the adoption of a novel detection scheme involving a position sensitive detector. These advances will mean that studies can be made in much greater detail at much higher-resolution than has been possible to date. A key area that these new capabilities will address is that of in the so-called mid-IR range in the cuprates (few hundred meV). Presently this is impossible to study with x-rays because of the presence of a large elastic line that obscures the weak inelastic signal out to several times the resolution half-width. With resolutions of ~50 meV, and better, that will be possible at NSLS-II, this difficulty will be overcome and it will be possible to study this important region for the first time. Several interesting phenomena occur in this energy range, including spin-waves and electronic excitations. Optical measurements that are confined to the center of the Brillouin Zone have revealed that sum rules in this spectral region are broken on going through the superconducting transition [3.5.4]. This in turn suggests that some of the condensation energy comes from a lowering of the kinetic energy of the electrons. However, these results remain somewhat controversial and poorly understood. Inelastic x-ray scattering will provide the first momentum-dependent information on this spectral region and may well be central to the problem of high-temperature superconductivity.

References

[3.5.1] H. Sinn, *J. Phys. Condens. Matter* **13** 7525 (2001).
[3.5.2] C.M. Wayman, and J.D. Harrison, *JOM* **41**(9) 26 (1989).
[3.5.3] M. Z. Hasan, et al. cond-mat/0406654.
[3.5.4] H.J.A Molegraaf, et al., *Science* **295** 2239 (2002).

3.6 Soft X-Ray Resonant Scattering: XRMS and RIXS

As discussed in Chapter 8, NSLS-II will be a superb source of soft x-rays. Conceptual designs for two beamlines are presented in Sections 11.7 and 11.8. These are optimized for high resolution and high flux, respectively. In this and the following section, we discuss some of the science drivers for these beamlines, beginning with the high-resolution beamline.

In the soft x-ray range, resonant processes at relevant core levels can enhance scattering amplitudes by orders of magnitude. Such resonant enhancements lie at the core of recent increased interest in the exploitation of soft x-rays for the investigation of wide classes of materials, including technologically relevant compounds and alloys and advanced nanoscale materials. Further, the wavelength of soft rays (~0.5 nm to a few nm) is well matched to many interesting and useful length scales, including those that occur intrinsically in many materials and those that have been engineered.

In particular, scattering studies in the soft x-ray range are uniquely suited to examining some of the most important issues surrounding correlated electron systems, spintronic materials, engineered ferromagnetic alloys, nanopatterned structures, advanced fuel cell electrodes, candidate hydrogen storage materials, and many other scientifically or technologically relevant materials. A large portion of the periodic table can be investigated via the use of soft x-rays, including the 3D transition metal L edges, rare-earth M4,5 edges, and the K edges of C, N, and O. There are strong resonant enhancements in the vicinity of these dipole-allowed absorption edges. In addition, polarization-dependent studies, which are more practical with advanced undulators and novel end station designs, can reveal underlying order in the charge, spin, and orbital degrees of freedom in the system.

X-ray Resonant Magnetic Scattering and Resonant Inelastic X-ray Scattering are two scattering techniques whose use in the soft x-ray range has increased considerably in recent years. XRMS and RIXS are both photon-in, photon-out techniques, and have a number of advantages over electron-based spectroscopies and scattering processes. For example, the probe depth of XRMS and RIXS is much longer because the measurements are not affected by the relatively short mean free path of electrons. Furthermore, photons are not affected by electric and magnetic fields and multiple scattering events are negligible in the soft x-ray range.

XRMS exploits magnetic sensitivity in diffraction patterns to extract element-specific information on magnetic ordering processes, on length scales from microns down to a few nm. While soft x-rays do not have the Q-range to probe the magnetic alignment of atoms in such structures and devices, the length scales of soft x-ray scattering are matched ideally to multilayer spacings, domain patterns, and feature sizes of current lithography techniques [3.6.1]; see, for example, Figure 3.6.1. XRMS is particularly well suited to studies of engineered thin films and multilayers, as the element-specific magnetism in individual layers can be separated. Indeed, the depth profile of the element-specific magnetic moment across an interface can be deduced from analytic models of specular and diffuse reflectivities [3.6.2].

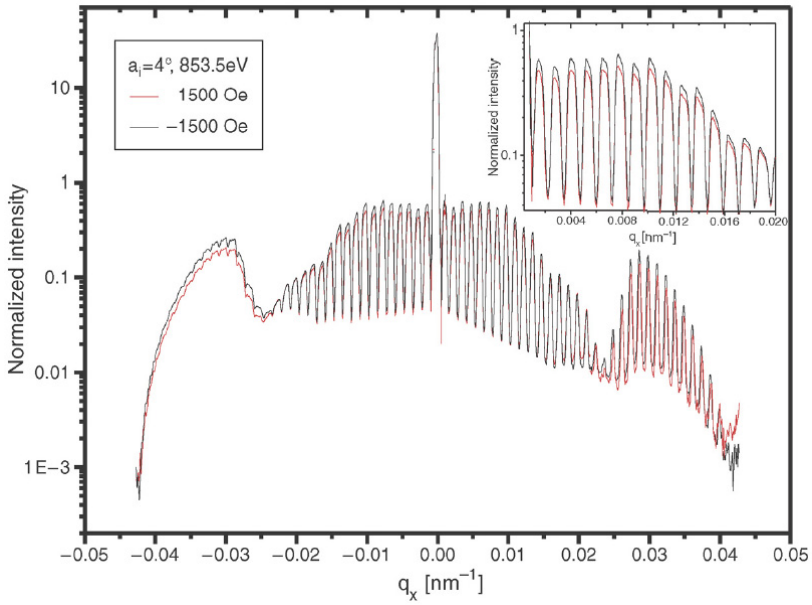

Figure 3.6.1 XRMS diffuse scan from an artificially structured magnetic micro-structure (FeNe alloy islands, 0.3×3 μm, 5 μm pitch). Note the large dynamic range of the scattering and the dozens of satellite reflections on either side of the specular peak. Source: [3.6.7].

The exceptional properties of NSLS-II will enable the implementation of soft x-ray beamlines with unsurpassed brightness, small photon spot size, energy resolution, and polarization control. These characteristics will be crucial in designing and ultimately using the next generation of XRMS and RIXS instrumentation. RIXS is inherently a very low-count-rate technique, and improvements in brightness and spot size translate directly to improved detection efficiency. In XRMS, the most valuable information is attained often only at high-momentum transfer or in off-specular scans. In both instances, the count rate at current instruments is often at the noise floor of the detectors.

In many complex oxides and intermetallic compounds, cooperative phenomena among the charge carriers result in charge, spin, and orbital ordering. Soft x-ray scattering is an ideal technique to study these ordered phases. For the transition metal oxides, XRMS in the soft x-ray range directly interrogates the valence states of the relevant transition metal d-orbitals and the oxygen s- and p-orbitals. Fractional order diffraction peaks in XRMS scans appear on the onset of orbital ordering. The peak intensity, which is correlated with the order parameter of the phase transition, can be measured as external parameters (e.g. fields, temperature) are manipulated [3.6.3]. In multi-layered structures of complex oxides, XRMS can probe interface-specific issues such as changes in the transition-metal valence state and modifications introduce by interfacial strain. Finally, careful modeling of XRMS scans can reveal unexpected phases that develop at interfaces, such as the development of anti-ferromagnetic insulating phases at the surface of otherwise metallic manganites [3.6.4].

Unlike XRMS, for which the energy of the scattered photons is not analyzed and hence only elastic scattering processes dominate the signal, RIXS directly examines inelastic processes by utilizing a soft x-ray spectrometer to resolve the energy of the emitted photons. The energy lost in the scattering process, which is measured in a RIXS experiment, can reflect important parameters such as the local partial density of states of an atomic species in a complex compound, low energy excitations (such as d–d interactions), and charge transfer from surrounding ligands.

As RIXS is an element-specific, local probe, it is an ideal technique to examine the low energy excitation spectra of correlated electron systems. As mentioned above, such systems are extremely sensitive to perturbations such as charge density, magnetic and/or electric fields, and temperature, particularly near phase transition boundaries. For example, in some “colossal magnetoresistance” manganites, at low temperatures the electron charge density self-organizes into stripe domains, resulting in a charge-ordered insulating phase [3.6.5]. Application of a magnetic field can drive such materials into a ferromagnetic metallic phase [3.6.6]. The mechanism governing the magnetic field–induced phase transition is thought to be increased

hybridization imposed by the alignment of valence spins; such a mechanism would change the valence structure of these materials. While such changes would be apparent in valence band spectra recorded with ARPES, the relatively large magnetic fields required (~several Tesla) preclude such measurements; such a limitation does not apply to RIXS. Furthermore, some degree of momentum resolution is available in RIXS, as the incident and emitted photon have well-defined directions and the projection of the momentum transfer can be varied by rotating the sample.

The momentum resolution combined with exceptionally good energy resolution of modern RIXS instruments will enable important and novel investigations into the still-unresolved mechanisms of high temperature superconductivity in cuprates. In such materials, the superconducting state at finite temperatures appears to be finely balanced with the competing dynamic stripe-order phase [3.6.6]. It has recently been suggested that spectral evidence of such dynamic stripe fluctuations might be accessible in momentum-resolved energy loss spectra [3.6.7] (see Figure 3.6.2). While the resolution required for such measurements is beyond the capacity of current-generation RIXS beam lines and spectrometers, the advanced capabilities of the NSLS-II XRMS/RIXS beam line, combined with a state-of-the-art RIXS spectrometer, will help unravel interactions between superconductivity and competing ordering phenomena in cuprates and related materials.

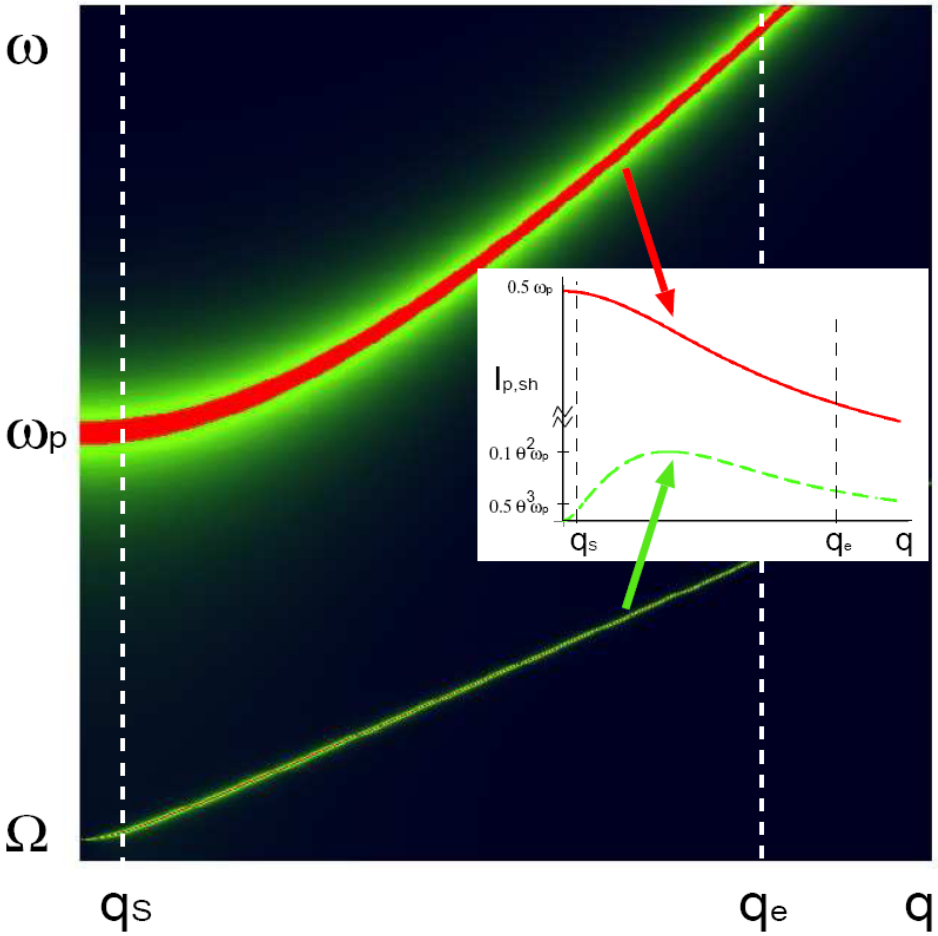

Figure 3.6.2 Electromagnetic absorptions in the "nearly ordered" superconductor, as seen by electron energy loss spectroscopy as a function of frequency Ω and momentum q. Besides the strong plasmon pole dominating the long wavelength dielectric response, the authors [3.6.7] also find a weak absorption that corresponds to the massive shear photon, giving away the presence of the "dual shear superconductor." This can be regarded as the unique fingerprint of a superconductor characterized by transient translational order extending over distances that are large, compared to the lattice constant. Tests of such theoretical predictions should be uniquely possible using resonant inelastic x-ray scattering at NSLS-II.

References

[3.6.1] A. Remhof, et al., Shining light on magnetic microstructures. *Superlattices and Microstructures* **37**(5) 353 (2005).
[3.6.2] S. Roy, et al., Depth profile of uncompensated spins in an exchange bias system. *Phys. Rev. Lett.* **95**(4) (2005).
[3.6.3] P. Abbamonte, et al., Crystallization of charge holes in the spin ladder of Sr14Cu24O41. *Nature* 1078 (2004).
[3.6.4] J.W. Freeland, et al., Full bulk spin polarization and intrinsic tunnel barriers at the surface of layered manganites. *Nature Mat.* **4**(1) 62 (2005).
[3.6.5] S. Mori, S. C.H. Chen, and S.W. Cheong, Pairing of charge-ordered stripes in (La,Ca)MnO3. *Nature* **392**(6675) 473 (1998).
[3.6.6] H. Kuwahara, et al., Spin-charge-lattice coupled phase transitions in bandwidth-controlled systems: (Nd,Sm)(1/2)Sr1/2MnO3. *Phys. Rev. B* **56**(15) 9386 (1997).
[3.7.7] V. Cvetkovic, et al., Observing the fluctuating stripes in high Tc superconductors. cond-mat/0607402 v1, 2006.

3.7 Soft X-Ray Coherent Scattering and Imaging

Like their counterparts in the hard x-ray region, soft x-ray imaging and coherent scattering are extremely photon-hungry techniques in which brightness is a crucial parameter. This is because such techniques utilize only the transversely coherent portion of the undulator beam, in both the vertical and horizontal planes. The high flux soft x-ray beamline, discussed in section 11.8, will produce a heretofore unprecedented (flux) × (energy resolution) × (spot size) figure of merit from 200 to 2200 eV in the soft x-ray range, with either fixed selectable polarization (linear, circular, or elliptical) or fast-switching between two selected polarizations. Figure 3.7.1 elucidates the high brightness of the EPU45 undulator beam by showing the number of transverse coherent modes it contains as a function of photon energy over the range to be covered by the high-flux undulator beamline. The number of modes varies from 3 at 200 eV to somewhat over 10 at 2 keV, where a single mode corresponds to a fully transverse coherent photon beam. This degree of transverse spatial coherence is very high, and in fact is more than ~10 times greater than competing synchrotron sources in the United States.

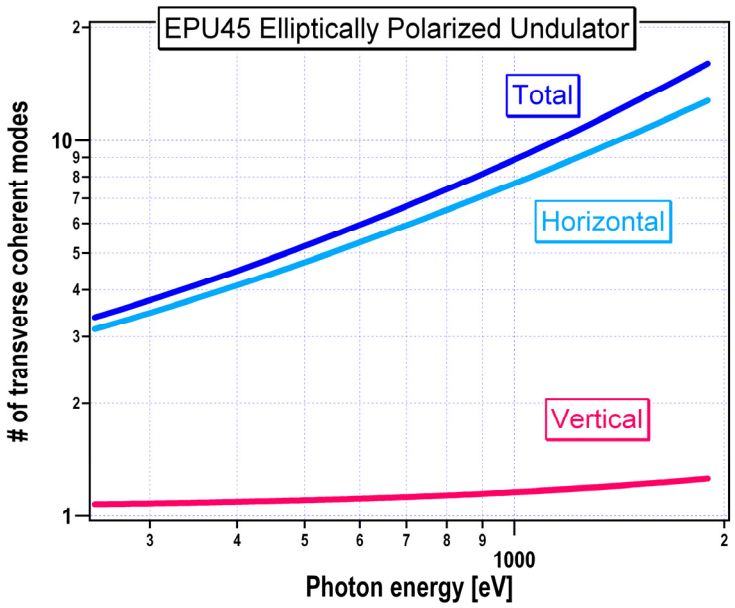

Figure 3.7.1 Coherent modes in the EPU45 beam. Vertical, horizontal, and total number of transverse coherent modes contained in the EPU45 beam as a function of photon energy.

These source properties, coupled with the state-of-the-art high flux soft x-ray beamline described in Section 11.8, will enable the next generation of experiments in soft x-ray microscopy and coherent scattering/imaging, i.e., those experiments that would suffer from impractically low signal rates using existing sources or are simply impossible, owing to the lack of selectable beam polarization. The types of scientific problems in coherent imaging/scattering to be addressed include nanoscale and mesoscopic imaging of noncrystalline samples (e.g., large cells and magnetic domains), time correlation spectroscopy of fluctuations in materials, and 3D imaging of granular materials. For soft x-ray microscopy, the problems to be addressed range from simultaneous spectroscopic (electronic) and microscopic (structural) measurements on nano- and mesoscopic length scales (e.g., of single nano-elements, nanocontacts, or nanomagnets), to understand isolated behavior and differences between boundaries/interfaces and bulk systems.

The design of the beamline described in Section 11.8 prioritizes photon flux over resolving power, in a tradeoff between transverse coherent flux and energy resolution or longitudinal coherence, the latter determining (among other things) the depth of field of a focused beam. The conceptual design has yielded a soft x-ray beam with, for example, a photon flux of a few × 10^{13} ph/s with a resolving power greater than 3000 for energies between 200 eV and 2.2 keV. By a simple change of grating, it can produce a flux greater than 10^{12} ph/s with a resolving power greater than 12000 over this photon energy range. In both cases, a focused 1-sigma spot size of 2.5 microns (H) by 1.3 microns (V) (see Figure 11.8.8) is achieved. Given the degree of transverse spatial coherence described above (~10 modes), the flux on sample for coherent scattering experiments will be in the 10^{11} to 10^{12} range, which represents a very significant improvement compared to existing U.S. soft x-ray coherence beamlines. For soft x-ray microscopies in which the beam is focused (e.g., with zone plates), if the efficiency of the focusing optic is on the order of 10%, we estimate a flux of 10^{10} to 10^{11} ph/s in the focused spot, which is again a quite significant improvement over existing soft x-ray beamlines. The extremely high flux-on-sample values described here will lead directly to reduced counting times, which currently limit the overall duration of soft x-ray coherent scattering/imaging and microscopy experiments. As described in Section 11.8, this may also drive the need for faster scanning stages in the case of scanning probe microscopies. Achieving significantly shorter measurement times for an image is also quite beneficial in minimizing nonstatistical fluctuations arising from unavoidable drifts in beamline or endstation components.

An example where this tremendous increase in coherent flux will have direct benefit is in the study of domain fluctuations in **c**olossal **m**agneto**r**esistance manganites. These materials are known to exhibit complex

low-temperature ground states in which the occupancy of the electronic orbitals varies from site to site in a periodic manner. These structures are known as "orbitally ordered." However, for reasons that are not at all clear, they do not attain long-range order at low temperatures, instead forming short-range ordered domain states. It is believed that the origin of these domains, and their dynamics, lies at the heart of the CMR phenomena. Very recently, coherent scattering has been used to observe the speckle pattern arising from these domains. Figure 3.7.2 shows one such pattern taken at ALS on beamline 12.0.2, utilizing the resonant enhancement at the Mn L-edge to give the scattering contrast for the orbital domains. The speckle pattern in Figure 3.7.2 was taken at low temperatures where the scattering is strongest; after binning, the count rate is approximately 50 counts per speckle.

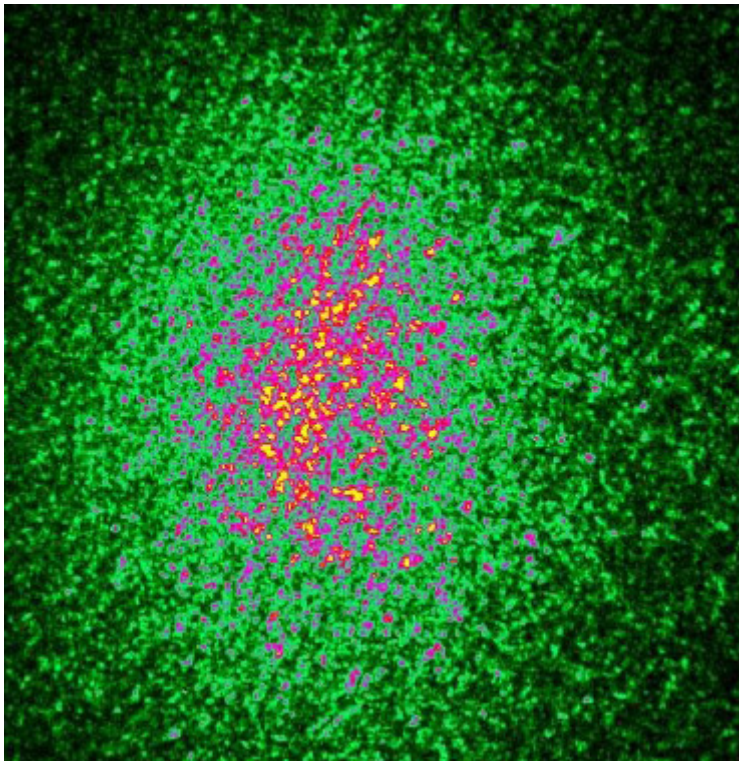

Figure 3.7.2 Speckle pattern from soft x-ray coherent scattering, from a sample with short-range orbital order. Data were taken at low temperatures at ALS [3.7.1].

Intensity corresponds to about 50 counts per speckle. Coherent intensities are expected to be a factor of 1000 higher at NSLS-II, allowing similar data to be taken close to the phase transition and the dynamics of the process to be studied for the first time.

At NSLS-II the coherent flux is expected to be 1,000 times larger; this will transform such experiments. In particular, it will become possible to make similar measurements close to the transition where the scattered intensity is very weak. Further, it should be possible to carry out XPCS measurements with such data, rather than the static measurements shown here, and study the dynamics of this important transition for the first time—an enticing prospect.

Finally, as stated above, the ability to select the polarization of the EPU45 photon beam adds an important variable to any of the experiments and techniques intended for this beamline. For tiny focused beams, the ability to select the polarization of the photon beam without altering its position or angle is crucial for any type of dichroism experiment (linear or circular) in order to illuminate only one selected spot on the sample. For magnetic-sensitive coherent scattering experiments, the ability to select the handedness of the beam polarization is essential, since the magnetization of the sample must remain fixed in order to avoid magnetization-induced changes to the domain structure of the sample and hence to the scattering pattern. The arguments for the advantages of fast-switching polarization capability are even greater, since the other experimental variables cannot be changed at the high rates necessary to detect tiny dichroic signals.

References

[3.7.1] J. Turner, K.J. Thomas, K. Chesnal, M. Pfeiffer, J.P. Hill, and S. Kevan, unpublished data.

3.8 Macromolecular Crystallography

Few fields have seen as dramatic an impact of synchrotron radiation as have the life sciences—in particular, macromolecular crystallography, where the technique has literally been transformed. Here we discuss the future impact NSLS-II will have on this surging field.

Understanding the living cell is the utmost challenge of modern biology. The expectation that a deeper understanding of the biological process can be achieved, once the three-dimensional structure of countless molecules and their functional roles have been conquered, is the driving force behind the revolution structural biology is undergoing today.

3.8.1 Macromolecular Crystallography Has Transformed Biology

Structural biology, perhaps especially x-ray crystallography, has transformed our understanding of biological processes. It was x-ray diffraction that provided the first clues to the structure of the DNA double helix 50 years ago. Nowadays numerous cellular mechanisms are described at a molecular level. Examples of these are protein synthesis, RNA transcription, DNA replication, immune response, enzymatic metabolism, signal transduction, cellular division, and the production of energy, to name just a few. In addition, structural biology has had a dramatic impact on the development of new drugs, wherein drug designers count upon being able to look in three dimensions at the molecular fit of their proposed drug into the active site of its target enzyme.

The principal tool to provide this knowledge for 25–30 years has been macromolecular x-ray crystallography (referred to as PX, the *P* for *protein*). New concepts and new equipment from many disciplines have provided a nearly exponential increase in productivity, as follows. Genetic engineering and protein cloning provide specimens. Crystal-growth screening methods and cryo-preservation improve this picture. Synchrotron radiation and the MAD method provide better data and a direct phasing vehicle. Modern detectors provide extremely accurate data very quickly. And finally, the computer industry's proven ability to obey Moore's Law lubricates the whole of this discipline. We're truly in a golden age for PX. Together these advances enhance two aspects of the research: increasingly difficult problems can be approached and solved with higher quality results, and human effort is decreased for each project, thereby making each individual more productive.

The growing use of synchrotron sources for macromolecular crystallography has increased the pressure on existing facilities to upgrade existing, or construct new, sources and beamlines. As of June 2006, more than three structures out of four deposited in the Protein Data Bank were solved using synchrotron data (see Figure 3.8.1), and this fraction keeps increasing. To some extent, the recent growth in structure depositions results from recent organized efforts in structural genomics. However, not only these projects, but also hypothesis-driven investigations launched by other structural biologists, or drug-target studies performed by pharmaceutical scientists, all benefit from the availability of brighter x-ray sources and the improved quality of instrumentation and methods that we see today. All of the power of the method has driven researchers to attempt increasingly difficult scientific problems, especially structures of large macromolecular assemblies and membrane proteins. Indeed, the size and complexity of macromolecules that can be studied has increased by an order of magnitude in the last roughly 15 years. There is no sign of this trend changing and it is certain that the brighter beams of NSLS-II will be in intense demand by this community to continue to push such developments.

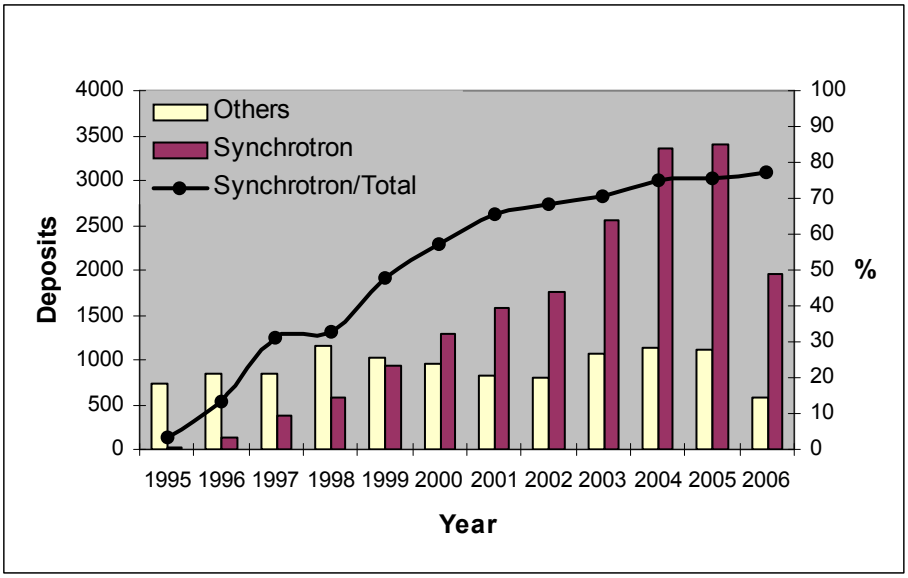

Figure 3.8.1 Evolution of Deposits to the Protein Data Bank (PDB).

Source: BioSync (http://biosync.rcsb.org/BiosyncStat.html)

3.8.2 The Most Difficult Problems Are the Most Interesting

These large structures represent the pinnacle of the structural biologist's craft. Picturing these large assemblies, firstly at the level of interactions among macromolecules, then at the level of atoms of the macromolecule interacting with a substrate, gives detailed information about the machinery of the cell. A great example is the three-dimensional structure of the bacterial ribosome, the protein synthesis apparatus of the cell, consisting of 150,000 atoms, in 53 proteins and three chains of ribosomal RNA, interacting with three tRNA molecules. Determination of this structure was an amazing *tour de force*. At least four major research groups used at least six synchrotron sources in multiple visits each to provide the model we have now of the whole particle and its two individual subunits [3.8.1–3.8.6]. Also in this category are the structures of virus particles, which have possible application in treatment of diseases and nanotechnology. These studies illustrate the difficulties of working with crystals in large complexes. Weak diffraction, close spacing of the reciprocal lattice, and radiation-sensitive crystals all conspired to make x-ray data collection possible only at synchrotron radiation sources.

The work on the voltage-dependent K^+ channel, for which Roderick MacKinnon, Rockefeller University, was co-awarded the 2003 Nobel Prize in Chemistry, is a perfect illustration of the exciting science obtained from structural studies on membrane proteins. Among other processes, these "life's transistors" control electrical activity in nerve and muscle. MacKinnon's work revealed a model for control of the passage of potassium ions through the pore in response to changes in cell membrane voltage (see Figure 3.8.2).

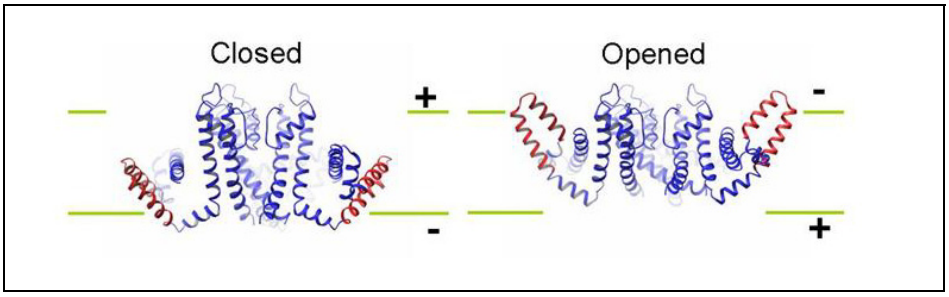

Figure 3.8.2 Model for control of potassium ions through a channel in the cell membrane, in response to changes in the cell membrane voltage. From the work of Prof. Roderick MacKinnon, Rockefeller University.

Membrane proteins perform many cellular functions and responses, representing about 30% of all proteins produced in a cell (making them quite interesting to the pharmaceutical industry). Although a number of investigators have reported structure determinations of macromolecular assemblies of membrane proteins, e.g., nutrient uptake across Gram-negative bacteria [3.8.7, 3.8.8], a serious impediment to all such work is that membrane proteins are notoriously difficult to produce and crystallize, providing small crystals that diffract poorly. To address this issue, structural genomics efforts specifically targeting membrane proteins have recently been launched. NSLS-II will provide the frequent access to a bright x-ray source required to solve these challenging problems.

3.8.3 NSLS-II Will Have a Major Impact on Structural Biology

There are numerous challenges in macromolecular crystallography that will benefit from NSLS-II. The two highest priorities are to handle very small crystals, and to treat very large molecular assemblies; this is where dramatic progress in structural biology will lie. Investigators in the Northeastern United States are at a serious disadvantage: neither the current NSLS, nor CHESS at Cornell University, can provide the small beam size with high intensity and excellent collimation that is required for this sort of progress. The ultrahigh source brightness of NSLS-II, in combination with anticipated developments in optics, detectors, and computing power, will allow structural biologists to tackle macromolecular assemblies of exceptional complexity, bringing our understanding of the macromolecular machinery of the cell to an unprecedented level. Also, in selected cases, time-resolved studies of macromolecular dynamics and interactions down to microsecond time scales or beyond will be possible, adding an additional dimension to the value of the results.

Many types of research effort will benefit. These will include small labs (ease of use, high-level staff support, training for inexperienced users), the large programmatic structure groups (rapid access, they take a role in planning and continued development of the facility, they will exploit new capabilities), the inventors of new methods (access for true experimentation, collaborations), and the pharmaceutical labs (automation, remote participation, efficient routine PX).

References

[3.8.1] Ban, et al., *Science* **289** (2000) 905.
[3.8.2] Harms, et al., *Cell* (2001) 107, 679.
[3.8.3] Wimberly, et al., *Nature* **407** (2000) 327.
[3.8.4] Pioletti, et al., EMBO **20** (2001) 1829.
[3.8.5] Yusupov, et al., *Science* **292** (2000) 883.
[3.8.6] B.S. Schuwirth, et al., *Science* **310** (2005) 827.
[3.8.7] Shultis, et al., *Science* **312** (2006) 1396.
[3.8.8] Pawelek et al., *Science* **312** (2006) 1399.

3.9 High Energy X-Rays

The use of high energy x-rays, defined here as those above ~50 keV, has grown in recent years to service what is now a diverse and continually growing community. As discussed in Section 11.12, the use of a 6 T wiggler source will provide a superb, intense source of x-rays out to 100 keV and beyond. Here we outline several possible programs that could utilize such a source at NSLS-II.

3.9.1 Earth and High-Pressure Science

The evolution of the Earth and other planets is a vast process lasting billions of years, involving huge amounts of materials (crystalline and molten silicates, metals, and volatile constituents), at temperatures from near absolute zero to several thousand degrees, and pressures from a fraction to millions of atmospheres. The present state of the Earth, as well as its evolution through time, is governed by the properties of these materials. Their properties at the relevant conditions of pressure, temperature, and stress dictate the red and blue regions of a seismic tomographic image (Figure 3.9.1), or control the depth and time history of earthquakes. These materials also define the frequencies of the oscillations of the Earth and the rate that plates slide over the surface. With the symbiotic development of synchrotron radiation and high-pressure techniques, experimental studies of such materials are experiencing an unprecedented surge of breakthroughs that were deemed inconceivable a decade ago. Synchrotron sources have fundamentally altered the nature of high-pressure experimentation, from reconnaissance study with limited capabilities to high-precision study with comprehensive material characterization over a wide range of pressures and temperatures. In particular, rheological properties, phonon-related properties, and the dynamics of chemical reactions can now be investigated at very high pressures and temperatures. By studying the materials of which the Earth is made, high-pressure research using synchrotron high energy x-rays has contributed significantly to understanding of the phenomena, processes, and state of the Earth. This information allows addressing issues that range from the chemical heterogeneity of the Earth's interior to the processes responsible for deep-focus earthquakes.

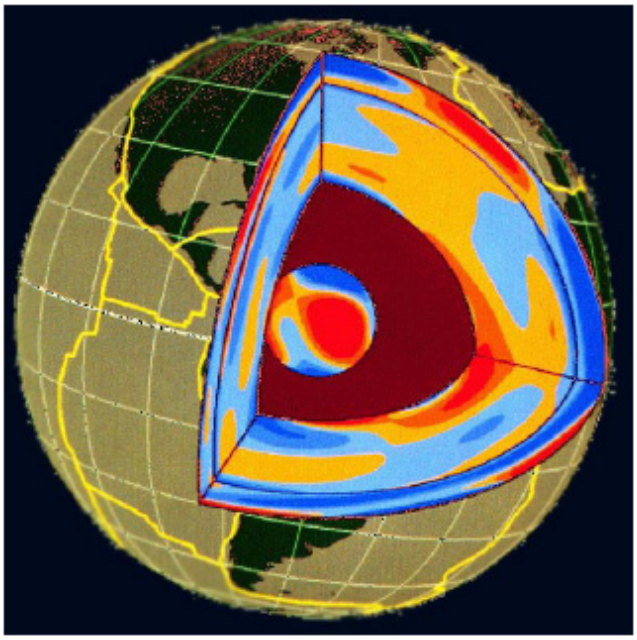

Figure 3.9.1 Seismologist's view of the Earth. Red regions indicate slow sound wave velocities, blue are fast. This structure may represent the flow patterns of hot (slow) material rising with sinking cold (slow) regions. Actual association of fast with either thermal or chemical variations requires high-pressure laboratory data.

3.9.2 Strain Mapping and Materials Science

Understanding and accurately calculating the stresses/strain field distribution is fundamental in the design engineering of static/cyclic load-bearing components. Often of equal importance, however, is the residual stress distribution that is present in the absence of external forces. Such residual can dramatically alter (for good or ill) a component's load capacity and resistance to failure. For example, compressive (tensile) surface stresses tend to retard (accelerate) the surface-initiation and growth of cracks. To compound the problem, the residual stress distribution is extremely difficult to experimentally characterize, offers little or no external evidence of its existence, and is often recognized only a posteriori, after failure.

The interaction between residual stresses (incurred during fabrication or duty-to-duty cycle fatigue) and applied stresses accounts for the failure of most structural engineering elements. However, many of the most

powerful techniques to probe this are explicitly destructive and involve theoretical modeling of the strain fields accompanying material removal (e.g., hole drilling and layer removal). Conventional x-ray and neutron scattering have traditionally been the only direct, nondestructive methods for strain profiling as a function of depth into a material. The short penetration depth of conventional x-ray analysis limits its use to the very near surface (<0.01 mm) region. The weaker scattering of the neutrons allows deep penetration (to tens of mm); however, it also precludes sampling volumes of less than about 1 mm^3. Thus, until recently there was a large hole in the spatial scale and resolution routinely accessible by direct/nondestructive methods of strain-field depth profiling (Figure 3.9.2).

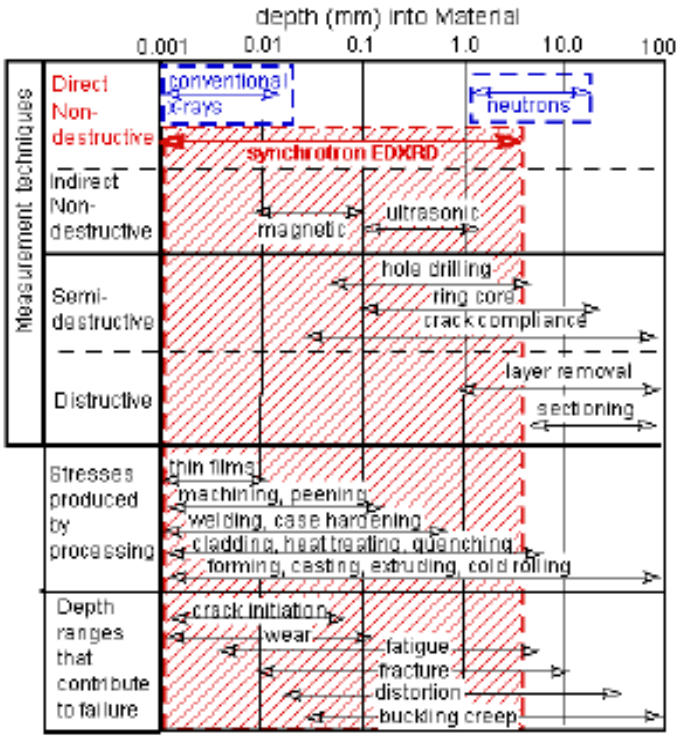

Figure 3.9.2. Residual strain (RS) sources, relevance, and means-of-measurement as a function of depth below the surface of a material. The summary is divided into: (top) the RS measurement techniques; the materials processing origins of RS (center); and the classes of material-component failure that can result from RS (bottom). The conventional x-ray and neutron scattering methods are indicated. The red-shaded region emphasizes the crucial range/relevance of high energy x-ray strain mapping.

In recent years, high energy synchrotron radiation x-ray diffraction techniques have emerged to fill this gap. These techniques have been applied to a number of problems, including applications to strain field mapping in the vicinity of fatigue cracks. High beam intensity has allowed the investigation of small diffraction volumes buried deep inside material specimens. At NSLS-II, one could create a 3D strain mapping facility that would be unique in the world.

Such a facility will have the capabilities to perform 3D strain mapping on large test specimens and actual components from real-world systems. Moreover, the ability to subject the specimens to large in-situ dynamic and static stresses, extreme temperatures, and corrosive/hostile environments will integrate into the facility. Specimens with the equivalent thicknesses (in terms of x-ray absorption) of 40 mm of steel will be strain mapped deep in their interior as well as on the surface. With this facility, the details of the residual, load-induced, and thermally induced strain distributions, as well as their interactions, can be mapped in three dimensions, bringing new insights into the failure modes of these components.

3.9.3 Medical Imaging and Radiation Therapy (MRT, DEI, and PAT)

Medical imaging and radiation therapy has a long tradition at the NSLS wiggler beamline X17B. At NSLS-II it will be possible to target specific techniques of synchrotron medical research that will reach the

stage of human studies in the foreseeable future, and could then be translated to clinical applications using bremsstrahlung sources. Examples include Microbeam Radiation Therapy, Diffraction Enhanced Imaging, and Photon Activation Therapy.

MRT is a major synchrotron medical tool developed at NSLS. Irradiation with arrays of parallel, very thin planes of x-rays was shown to be tolerated by normal tissues, including the central nervous system, at very high doses of up to several hundred Gy. MRT beam arrays were also shown to preferentially damage tumors when used at very high doses. Although the underlying mechanisms of MRT effects are not well understood, they clearly involve the recovery of both the microvasculature and the glial systems. In particular, microvasculature repair seems to be facilitated by endothelial and other support cells surviving between the individual microbeams. The method, developed in early the 1990s at the NSLS X17B1 superconducting wiggler, has also been pursued since 1996 at ESRF. Recent studies indicate that the tissue-sparing effect of microbeams stays strong with beams as thick as 0.68 mm. The study also showed that MRT could be implemented by using two arrays of parallel thick-beams aimed at the target from perpendicular angles to interlace, producing a nonsegmented solid beam at the target while exposing the surrounding healthy tissues only to microbeams (Figure 3.9.3).

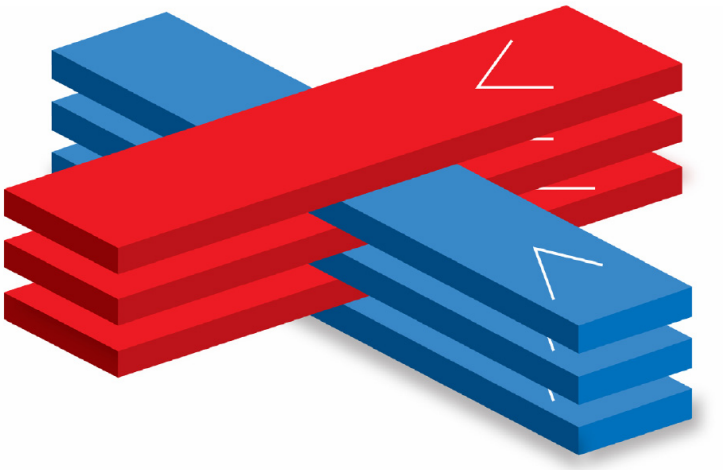

Figure 3.9.3 Model of Microbeam Radiation Therapy (MRT). Interlaced microbeams produce an unsegmented beam in the target but spare surrounding tissue.

MRT at NSLS-II will benefit from the beam's high energy and high intensity, which are essential to allow the beamline to be used for clinical studies. In particular, the beamline will make possible the use of a heavily filtered beam (e.g., one with a half-power energy of 150 keV to improve dose penetration) at a dose rate of 2000 Gy/s. This dose rate will allow the delivery of a therapeutic dose (e.g., 200 Gy incident dose) in a fraction of a heartbeat. The current X17B1 beam provides about 40 Gy/s at 12 keV half-power energy. Another major advantage of an MRT setup at NSLS-II will be the ability to allow for implementation of clinical MRT, accommodating all auxiliary functions, such as the physician's control area and medical imaging for patient positioning into the beamline infrastructure.

Diffraction Enhanced Imaging is another method developed at NSLS. DEI's angular sensitivity enables the gradient of the x-ray index of refraction to be measured, as well as the yield of "small-angle scattering" (extinction contrast). In DEI, a collimated monochromatic x-ray beam is passed through the subject as in conventional radiography. A silicon crystal (analyzer) is placed between the subject and the detector. The analyzer discriminates small-angle x-ray scattering and introduces sensitivity to refraction occurring within the subject. Variations in the subject's density and morphology refract the x-rays, generally in the sub-microradian range. The analyzer converts these subtle angle variations into intensity variations. Thus DEI enhances soft-tissue imaging, which lacks contrast in traditional x-rays and CT. DEI at NSLS-II will benefit from the beamline's high beam energy and intensity that could be used to image subjects as large as a human

head in a reasonable time in the CT mode, using beams of about 60 keV. This kind of work is impossible for implementation at the current NSLS.

Photon Activation Therapy was also developed at NSLS. PAT is based on the principle that absorption of radiation dose in tissue can be enhanced by administering contrast agents, including heavy elements, to the tissue and then irradiating the tissue with an X-ray beam in which the energy spectrum is concentrated above the K-edge of the contrast element. Inducing a photoelectric effect in a stable high Z atom localized to tumor cell DNA generates the emission of short-range, low energy Auger electrons that act like an energy sink in the DNA, severely damaging both strands, and so increasing the effective radiation dose to tumors**.** Such damage is associated with significantly less repair than single-strand breakage. The biological efficacy of Auger electron emission induced by synchrotron radiation was reported in PAT studies with iodine. The method can also be used with agents that do not target the cell nucleus, to enhance the dose localization in the target.

3.10 Hard X-Ray Imaging

X-ray imaging covers a wide range of techniques and applications and is likely to be among the most prominent techniques in use at NSLS-II. It is impossible here to do justice to the breadth of science that may be covered—ranging from materials science, to life science, to nanoscience. Here we simply mention a few of the techniques that will be utilized and list some likely applications. At NSLS-II, x-ray imaging might be expected to focus on the following core experimental techniques: 1) phase-contrast imaging, in both static and time-resolved modes, 2) diffraction-enhanced imaging capability, 3) coherent Fresnel diffraction imaging, and 4) image retrieval and tomographic 3D reconstruction as an integral part of the facility.

A good portion of the scientific program requires a highly coherent x-ray beam in an energy range of 7–50 keV, and a large field of view with minimal source-size smearing. In addition, time-resolved imaging experiments could make use of the pulsed nature of the NSLS-II synchrotron x-rays with an aim to achieve a single-pulse temporal resolution of ~50 ps and a simultaneous high spatial resolution of ~1 μm.

3.10.1 Phase-Contrast Imaging (PCI)

Phase-contrast x-ray imaging is a coherence-based technique that makes use of the edge-enhanced effects in near-field Fresnel diffraction and allows detections of weakly absorbing features in a specimen that are not observable in conventional absorption-based x-ray radiography. The spatial resolution with PCI is generally limited by the detector spatial resolution of 1–10 μm, which is well suited for many biological, medical, and materials science applications. A KB mirror system is planned to provide a projection-imaging capability that will allow increased spatial resolution down to 0.1–1 microns, if necessary.

Phase sensitivity directly depends on the distance between source and specimen, and between specimen and detector, thus leading to the requirement of a long beamline for PCI applications. In addition, a long beamline provides an unobstructed larger field of view, which will be needed for imaging larger specimens in materials and medical sciences. Based on the designs and experiences of the existing synchrotron beamlines in the world, a 300 m beamline at NSLS-II will provide a phase sensitivity of 2 mrad within the typical spatial resolution of 1 μm, and will be able to detect minute refractive angular deviations of <1 μrad. These specifications will represent the state-of-the-art in worldwide x-ray PCI capabilities.

Phase contrast imaging will be the workhorse facility of the XRI beamline, perhaps contributing to 60 to 70% of scientific research. Examples of research include: fracture mechanics of composites and biological materials, materials microstructure/properties such as deformation and sintering; bone and cartilage growth and formation; small animal and soft tissue research on vascular and pulmonary functions; porosity distribution in foods; structure and development of plant seeds; characterization of geological structures and microfossils; cement mortar research; structure and development of foams; granular packing of non-

equilibrium systems; time-resolved studies of internal complex fluid flow and fluid sprays; and multi-phase fluid flow using particle image velocimetry.

3.10.2 Diffraction Enhanced Imaging

Diffraction enhanced imaging, discussed above in the context of high energy x-rays, makes use of a high quality crystal analyzer to detect refracted or small-angle-scattered x-rays from the specimen. Because of high angular selectivity of the crystal analyzer, DEI can image very minute phase shifts due to density inhomogeneity in the specimen. In addition, in ultra-small-angle-scattering (USAXS) mode, it can be used to image density inhomogeneities and fluctuations at a given spatial frequency of interest. Technically, DEI can be set up in one or all of three regimes: a) top of analyzer rocking curve for scattering background rejection, b) side of analyzer rocking curve to convert refraction-angle into intensity contrast, and c) far from analyzer rocking curve on direct beam to pick up USAXS signals at a given scattering angle. Examples of DEI applications include: microstructures and defects in materials; deformation, sintering, and crack formations; porosity in bones and calcification effects; soft tissue and vascular network detections in x-ray radiographs; and diagnosis of cancerous tumors in soft tissues.

3.10.3 Coherent Fresnel Diffraction Imaging (FDI)

Coherent Fresnel diffraction imaging involves collecting Fresnel or in-line holograms in near-field regimes and reconstructing original nonperiodic objects by image retrieval techniques. Compared to PCI, discussed in 3.10.1, coherent FDI seeks to record a complete set of Fresnel diffraction fringes at a greater detector-to-specimen distance, which allows quantitative determination of an object's density function and permits spatial resolution reaching well beyond the detector pixel resolution. When working in the intermediate regime of a few Fresnel zones, FDI essentially becomes the far-field coherent diffraction imaging technique, as discussed in Section 3.2. Examples of potential applications include: structures of large biological functioning units (e.g., tissues, myocytes, muscles, bones, cartilage, etc.); identification of organelles and critical protein assemblies in biological cells; self-assembly of macromolecule arrays with nanotemplates and nanogrids; structural imaging of multi-unit inorganic/small-molecule/biomolecule composites; noncrystalline nanoparticles such as nanoclusters and nanowire assemblies; structural imaging of precipitates and defects in engineering materials; and topographic imaging of domain growths in ferroelectrics.